TECHNISCHE UNIVERSITÄT WIEN

Diplomarbeit

Synthetic approaches to novel crystalline sponges

Ausgeführt am Institut für angewandte Synthesechemie
der Technischen Universität Wien

Unter der Anleitung von
Priv.Doz Dipl.-Ing. Dr.techn. Peter Weinberger

durch
Martin Gollowitzer
Pickgasse 5/35
1100 Wien

15. August 2017   Unterschrift (Student)

Abstract

The crystalline sponge method, invented by the Fujita group at the University of Tokyo in 2013 allows to analyse the structure of non-crystallisable compounds by single-crystal X-ray diffraction through inclusion of them as guest molecules within a metal-organic framework. Since we assume that the ligands known to the literature do not produce cavities large enough to incorporate tetrazole-based iron(II) coordination complexes that act as spin-crossover materials and which we want to analyse with this method, the need for a novel ligands to build up the MOF arises.

Therefore, novel ligands that supposedly increase the size of the cavities for the guests within the host structure were synthesised. Two out of four candidates where successfully produced. One of the two ligands formed a one-dimensional coordination polymer structure with $ZnCl_2$.

Crystal structures of the ligand and the coordination polymer were elucidated by single-crystal X-ray diffraction.

Zusammenfassung

Die 2013 von der Forschungsgruppe um Prof. Fujita an der Universität von Tokio entwickelte „Crystalline sponge"-Methode erlaubt die Analyse der Struktur nicht-kristallisierbarer Stoffe mittels Einkristall-Röntgendiffraktion, indem diese in einer metallorganischen Gerüststruktur (metal-organic framework, MOF) als Gastmoleküle eingebaut werden. Da die in der Literatur für die MOF-Struktur verwendenten Liganden unserer Annahme nach zu kleine Poren in der Gerüststruktur erzeugen, um Tetrazol-basierte Eisen(II)-Koordinationsverbindungen, die als Spin-Crossover-Materialien fungieren und von uns mittels dieser Methode analysiert werden sollten, einzubauen, entstand die Notwendigkeit für neue Liganden.

Aus diesem Grund wurden neue Liganden, die vermutlich größere Poren erzeugen sollten, synthetisiert. Zwei der vier zuvor identifizierten Kandidaten wurden erfolgreich hergestellt. Einer der beiden Liganden bildete mit $ZnCl_2$ ein kristallines eindimensionales Koordinationspolymer.

Von besagtem Liganden und dem Koordinationspolymer wurden Kristallstrukturen mittels Einkristall-Röntgenbeugungsanalyse gemessen.

Acknowledgements

First of all, I want to thank my supervisor Priv.Doz. Dr. Peter Weinberger for giving me the chance to conduct my master's thesis in his group and all the support and motivation he has given me throughout my work. A special thanks also goes to my colleagues in the research group for the synthetic expertise that they shared with me and all the measurements they did for me.

Furthermore, I want to thank my colleagues and friends at the other inorganic chemistry groups of our institute for many interesting discussions and all the fun we had together. Thank you also especially to Priv.Doz. Dr. Berthold Stöger for introducing me to the miracles of single-crystal X-ray diffraction and for his endless patience while explaining me the structures of my compounds.

Another big thank you of course goes to my family, especially my parents for their love and support through all my life, to my brother Stefan for his unalterable believe in my skills and to my nieces Anna and Paula for their smiles – they kept me going.

Most importantly however, I want to express my deep gratitude to Barbara, my wife. Thank you for your unconditional love and for everything you did for me.
I look at you and smile because I'm fine.

Contents

List of Figures

List of abbreviations

ATR	attenuated total reflectance
BTETP	4',4'',4'''-(1,3,5-Benzenetriyltri-2,1-ethynediyl)tris-pyridine
CCDC	Cambridge Crystallographic Data Centre
DCM	dichloromethane
EE	ethyl acetate
h	hour
HPLC	high-performance liquid chromatography
IR	infrared
MeOH	methanol
min	minute
MOF	metal-organic framework
MS	mass spectrometry
n-BuLi	n-buthyllithium
NMR	nuclear magnetic resonance
PE	petroleum ether
ppm	parts per million
THF	tetrahydrofurane
TLC	thin-layer chromatography
TPT	tris(4-pyridyl)-1,3,5-triazine

1. Introduction

Chemistry is known as the science dealing with the composition, structure, properties and interconversion of molecules and different forms of matter [1–3]. Therefore, one of the most important tasks for chemists is the proper identification of the compounds that they are working with.

In the early times of modern chemistry, only few methods (*e.g.* volumetric and gravimetric analysis) were available and therefore, chemists had to use very little information and apply logic to find out what the molecules they were examining looked like. Today, the number of methods at the chemists' hand is much bigger and the amount of information we can retrieve from them is enormous. However, while methods like multi-dimensional nuclear magnetic resonance spectroscopy, Fourier-transform infrared spectroscopy, neutron activation analysis or high-performance liquid chromatography coupled with high-resolution mass spectroscopy have massively increased the speed at which newly synthesised or discovered compounds are identified, they still do not provide us with the absolute structure of compounds at the atomic level.

To date, single-crystal X-ray diffraction is the method of choice to gain this kind of information. While it has become part of the routine analysis for many chemists, it still has – as the the name already implies – the intrinsic limitation that it can only be applied to substances that can be crystallised in an ordered fashion.

In 2013, the research group of Makoto Fujita published a new method [4] that allowed to overcome this limitation at least for small organic molecules and at the same massively reduced the amount of analyte needed to the nanogram scale. The idea behind the concept that was later called the "crystalline sponge method" [5] is to embed the molecule of interest in a three-dimensional coordination network or *metal-organic framework*, giving it a far-range order and thereby making it accessible to single-crystal X-ray diffraction. As opposed to similar methods published earlier, this method does not require co-crystallisation of the analyte and the host.

Due to the background of our group in researching iron (II) spin-crossover compounds with tetrazole-based ligand systems [6–10], the problem of non-crystallisabilty is well-known to us, as quite a few tetrazole coordination complexes of iron (II) are hard or impossible to crystallise. While the host framework described in the original publication [4] does not strictly limit the size of the guest molecules [11], coordination complexes of this kind are clearly too bulky to penetrate the voids of this metal-organic framework. Therefore, this work aims at adapting the original crystalline sponge $\{[(\mathrm{ZnI_2})_3\mathrm{TPT_2}] \cdot x\,(\mathrm{solvent})\}_n$ (TPT = tris(4-pyridyl)- 1,3,5-triazine) for bigger guest molecules in order to obtain crystal structures of this kind of materials.

2. Crystalline sponges

In 2013, the research group of Makoto Fujita at the University of Tokyo published a novel method [4] for analysing non-crystallisable compounds with single-crystal X-ray diffraction. This method of "crystal-free crystallography" [12], later referred to as "crystalline sponge method" [5], was considered a ground-breaking development as it clearly had the potential to revolutionise many fields of science that suffer from the intrinsic limitation of single-crystal X-ray diffraction imposed by the need of crystalline samples. Despite having some problems with the data quality in the beginning [13], the method has since been proven to work and the number of publications with applications of it has increased over last years.

2.1. History
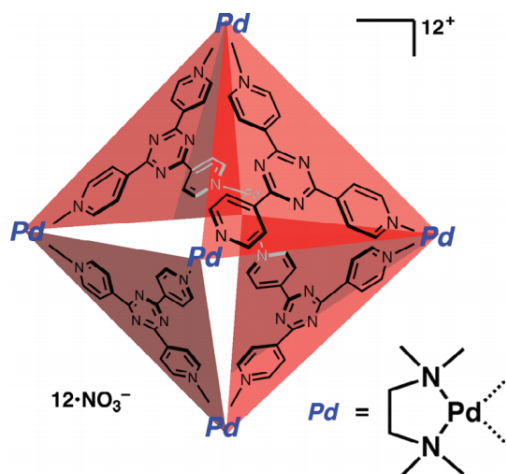
Figure 2.1.: Schematic representation of a discrete cage formed from TPT with Pd^{2+} ions [14, 15]

In 2002, Biradha and Fujita discovered that a metal-organic framework assembled from tris(4-pyridyl)-1,3,5-triazine (TPT), a panel-like ligand that was known to form container compounds with Pd^{2+} [14] (*cf.* Figure 2.1) and three-dimensional networks with Cu^{2+} [17],

and ZnI_2 could absorb and release solvent molecules (*cf.* Figure 2.2), expanding and contracting in a crystal-to-crystal manner [16].
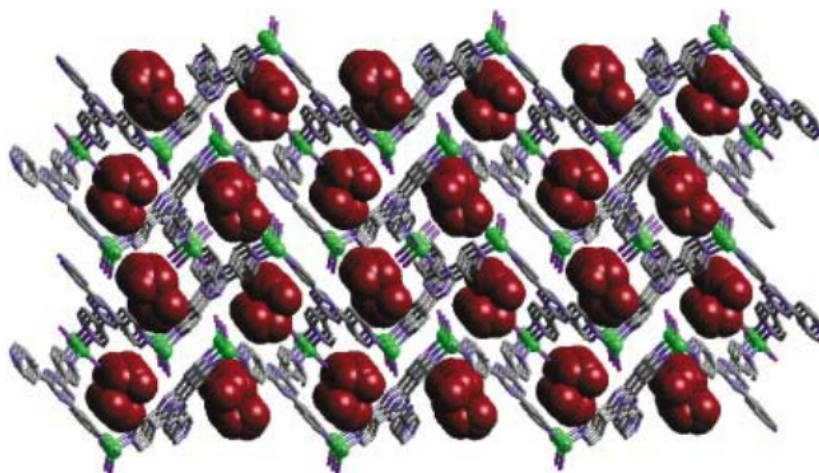
Figure 2.2.: Bromoform molecules (brown) interpenetrating a three-dimensional network built up of TPT and ZnI_2, forming a complex of the form $[\{(ZnI_2)_3(tpt)_2 \cdot 2\,CHBr_3\}_n]$ [16]

Since the solvent molecules interpenetrating the three-dimensional network were very small, there was no immediate use case for this discovery. Because of that, the research group worked on adapting the approach to allow the take-up of large organic molecules into the MOF. They reported successful inclusion of molecules like anthracene and perylene two years later [18]. In 2005, they reported a biporous material built up from the same three-dimensional network by addition of triphenylene, in which two cylindrical channels showed selective absorption of preferred solvents from a mixture [19]. A few more years later, Inokuma *et al.* reported that networks built up of TPT and $Co(NCS)_2$ (*cf.* Figure 2.3) showed similar guest-inclusion behaviour [15].

Finally, in 2013 the Fujita research group reported the first application of porous metal complexes or "crystalline sponges" for the structure determination of organic molecules [4]. While the inclusion of the molecule of interest in a host material was not particularly new – small guest molecules had been studied in clathrates before [20–22] – the application of metal-organic frameworks as specific host materials definitely was. Prior to this new application, MOFs had mainly been used in applications such as gas separation and storage
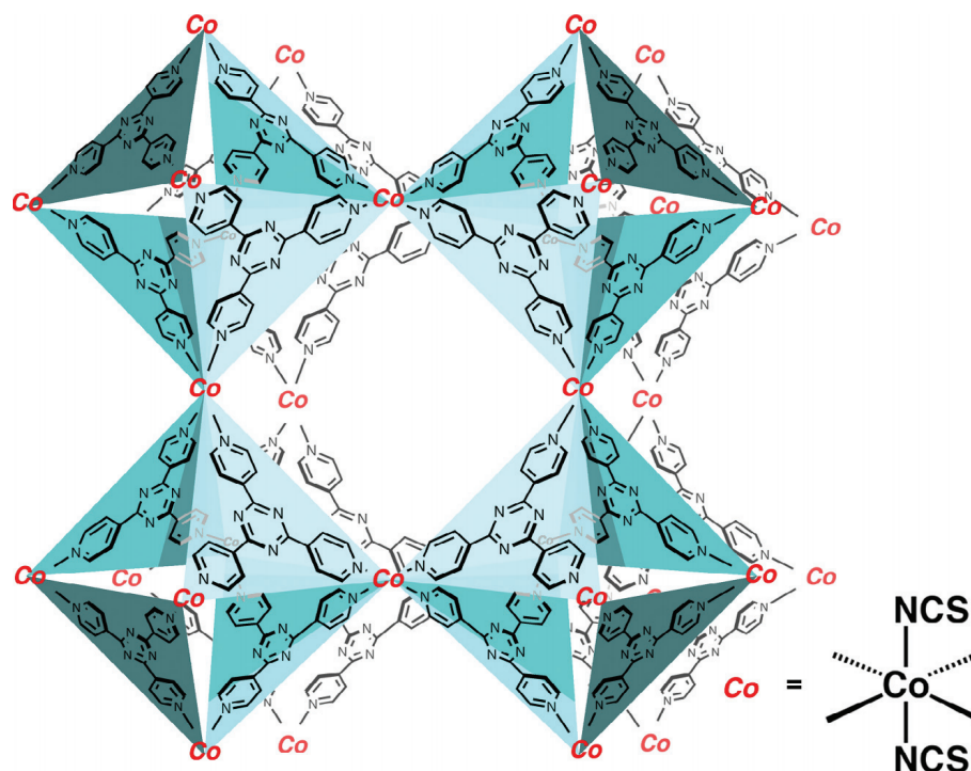
Figure 2.3.: Schematic representation of network complex
$\{[Co(SCN)_2)_3(tpt)_4]\cdot x(Guest)\}_n$ [15]

or catalysis, among others [23]. In their report, Inokuma *et al.* used both the ZnI_2-based as well as the $Co(NCS)_2$-based MOF they had reported on before. Because of the possibility to soak the sponges in a solution of the molecule to be incorporated instead of the neat analyte, the absolute amount of the molecule of interest necessary to perform the analysis was reduced to the nanogram range. This fact immediately suggests the application of the method for natural compounds that often can only be isolated in very low amounts.

Of course the new method was not perfect from the beginning and one part of the results of the first publication had to be revised later, because one stereogenic centre had been assigned wrongly due to the low quality of the crystallographic data [13]. Despite the criticism following the corrigendum [24, 25], the method was proven to work independently by other groups shortly after the initial publication [5, 26, 27], whereas the Zn-based MOF turned out to be favoured by the scientific community. A more detailed description of the

procedure [28] as well as a report on general improvements of the method [11] were publish by the Fujita group later on.

Especially, the structural investigation of natural products has turned out to be an important application of the method [29–31], revealing structures that scientists had been unable to elucidate for decades in some cases [32]. In 2014, Yasuhide Inokuma received the Chemical Society of Japan Award for Young Chemists for 2013 [33] for his work on the crystalline sponge method.

2.2. Advantages and limitations

While the abolition of the need for crystalline samples clearly is the most obvious advantage of the crystalline sponge method, other aspects of the technique are also worth noting. Especially, the fact that the amount of analyte required to perform the X-ray diffraction experiments can be drastically reduced is a major advantage of the method. Due to the fact that crystalline sponges can be soaked in a solution of the analyte as long as the solvent is not a very good one (which would retain the analyte from entering the pores), a sub-microgram amount of the molecule of interest can be enough for its structure to be elucidated.

Unfortunately, these positive aspects of the technique come at a price (as is the case for any analytical method). Due to the low amounts of sample that actually get soaked into the crystal, the purity of the compound in question is very important. However, purity is also a requirement for "normal" single-crystal X-ray diffraction. This limitation can, however, be overcome by coupling the crystalline sponge method with high-performance liquid chromatography. The fractions collected from HPLC can directly be used for the soaking step as long as the solvent used in the chromatography is not too good.

Despite that limitations above, there are a few more requirements for the host framework to be usable as a crystalline sponge. First of all, the ligands used to build up the metal-organic framework must in no way undergo reactions with the analyte. While this requirement is rather obvious, it still is very important to consider.

Secondly, the pores in the framework should have low symmetry. Highly symmetric pores allow the guest molecules to arrange in different ways within the pore, thereby leading to disorders which cause drastically lower data quality.

Another important aspect is the size of the pores in the host, which should fit the size of the analytes. If the pores are too big, this again leads to disordered guest molecules, reducing the data quality.

Despite the limitations above, the crystalline sponge method does of course also suffer from problems common to any kind of crystallographic analysis like symmetry problems and the information obtained from it needs to be combined with data received from complementary methods like mass spectrometry [4].

2.3. Applications and recent developments

After the initial publication, the Fujita group started cooperations with numerous other research groups worldwide, analysing samples for them [34].
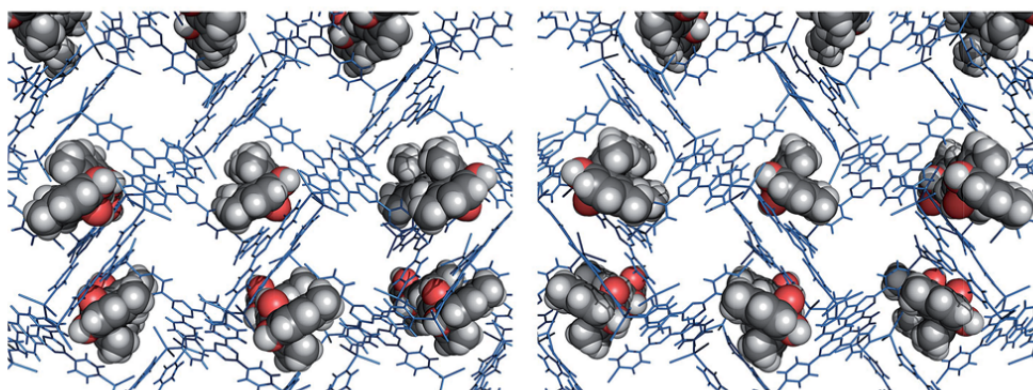
Figure 2.4.: Network structure of the two enantiomers of an axially chiral *o*-substituted biaryl encapsulated in a crystalline sponge [35]

In 2014, the crystalline sponge method was already used by Ikemoto *et al.* [36] to investigate the reaction mechanism of a Pd-catalysed aromatic bromination within a crystalline sponge by time-dependent X-ray diffraction. They were able to observe an intermediate species that is normally not accessible due to very fast dimerisation.

In 2015, Yoshioka *et al.* for the first time used the crystalline sponge method to determine the absolute structures of compounds with axial (*cf.* Figure 2.4) and planar chirality, devoid of the need for crystallisation or derivatisation of the examined compound. This clearly showed that the method can also be of great use in the field of asymmetric synthesis.
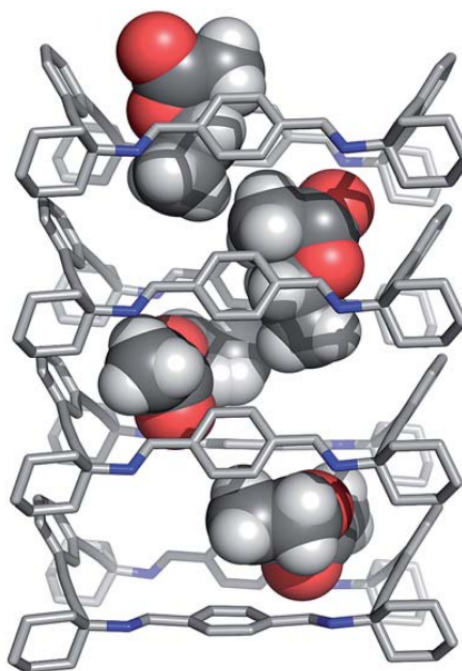
Figure 2.5.: Crystal structure of a non-MOF crystalline sponge holding ethyl acetate in its channels [37]

The success of the crystalline sponge method also inspired others to develop materials for guest inclusion and so Sanna *et al.* [37] published a crystalline sponge which consists of a porous organic material based on dispersive forces (*cf.* Figure 2.5). The advantage of such a system is the absence of heavy atoms like I or Br, which strongly contribute to the overall diffraction pattern because of their electron-richness. Around the same time, a chiral metal-organic material (CMOM) using Co(II) as the metal centre and 4,4'-bipyridine and mandelate as the ligand system was investigated for the application of resolving racemic mixtures [38].

Ramadhar *et al.* contributed to the method by publishing general guidelines after using the method with synchrotron radiation [27] as well as investigating the effects of changes in

the terminal ligands, replacing I with Br and Cl [26]. They found that the "empty" sponges had the same space group independent of the used Zn salt, but there was a difference in the unit cell expansion during the soaking step. Further improvements towards a broader use of the method through adaptions of the protocol came from Waldhart *et al.* [39]. They especially highlighted the robustness of their adapted method to user error.

In 2016, Brunet *et al.* faced unexpected results in the preparation of the cobalt based crystalline sponge when trying to apply the crystalline sponge method on magnetic molecules. Because of that, they decided to examine the transformations that the MOF underwent during the soaking. Thereby, they discovered a change in the coordination sphere of the Co(II) ions on the surface of the crystal [40].

In the same year, pharmaceutical researchers from China used crystalline sponges based on ZnI_2 and $ZnBr_2$ in combination with high-performance liquid chromatography to characterise volatile compounds from essential oils, showing that coupling of these methods could provide a platform for gaining information about closely related isomers [41].

Also in 2016, novel metal-organic frameworks that act as crystalline sponges were developed using Aluminium [42] and Zirconium [43] (*cf.* Figure 2.6) as metals.

A study by Hayes *et al.* [44] investigated the reproducibility of aromatic guest inclusion and the host-guest as well as guest-guest interactions within the crystalline sponges developed by Inokuma *et al.* The results showed a dominant role of π–π and CH–π interactions for the ability of the crystalline sponge to order the guest regularly. In another publication the same group focused on the intermolecular interactions of molecules encapsulated in a crystalline sponge, giving an insight on guest behaviour within the MOF [45].

Another success of the original crystalline sponge method was reported by Duplan *et al.* [46], who were able to reveal the structure of intermediate adducts in a Michael addition between thiol nucleophiles and cyanoenones that had previously been detected by NMR, UV/Vis spectroscopy and MS in solution, but which had never been isolated. The fact that reactions can be run within molecular flasks by first encapsulating a substrate in a crystalline sponge and then treating the crystal with a solution of the reagent of choice expands the potential field of applications even further, as in-situ X-ray measurements
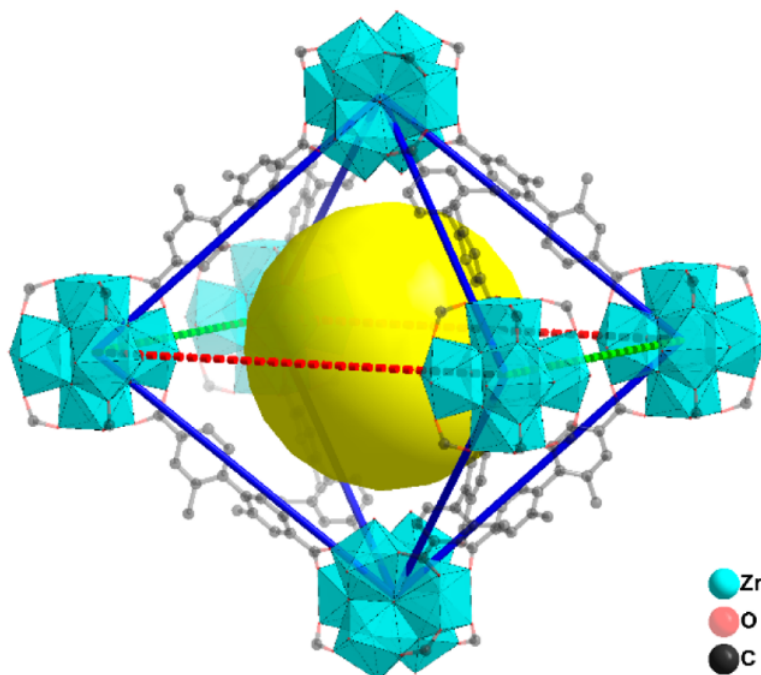
Figure 2.6.: A zirconium-based MOF that can act as a crystalline sponge [43] (hydrogen atoms omitted for clarity)

can potentially aid the revelation of reaction mechanisms in organic chemistry. Another example for reaction mechanism elucidation was given by Cuenca *et al.* [47], demonstrating the *syn*-addition mechanism of metal-free diboration, which previously had only been examined by indirect means.

Unrelated to the original use as a crystalline sponge, Brunet *et al.* investigated the magnetic properties of the $Co(SCN)_2$-based MOF used in the original paper by Inokuma *et al.* [4], showing that this sponge is the first three-dimensional network built from Co(II) single-ion magnets [48].

In summary, the applications of the crystalline sponge method spread across many fields of research, from plain X-ray diffraction of non-crystallisable compounds to coupled methods with chromatography of volatile compounds to reaction mechanism investigation. Nonetheless, the method cannot be called widely adopted, as its application requires lots of experience and finding the right conditions for soaking of the guest molecules can be cumbersome. This is the reason why the inventors of the method refrain from commercial-

ising the method until it has become more convenient. This decision is remarkable insofar as the Fujita group actually does cooperate with big pharmaceutical companies [34]. Time will show whether the method will really be able to revolutionise structural investigations, especially in regard of compounds exceeding the size of simple organic molecules.

3. Aim of this work
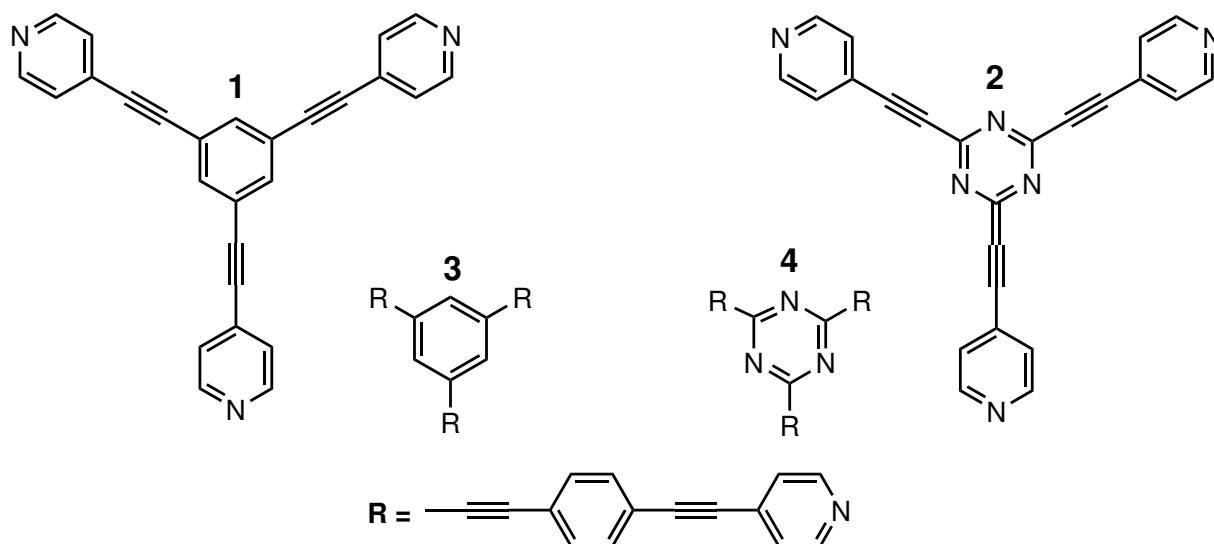
Figure 3.1.: Candidate ligands for crystalline sponges with extended pores, bearing benzene (left) and 1,3,5-triazine (right) as central aromatic ring system

While the original crystalline sponges introduced by Inokuma *et al.* have a certain amount of flexibility regarding the size of their possible guests [11], they are still limited to incorporating rather small organic molecules. With iron(II) spin-crossover compounds based on substituted tetrazole ligands being one of the main fields of research in our group, the problem of hard to crystallise compounds is a common one, as especially coordination complexes with group 14-substituted tetrazoles [6] are often oily. This makes the crystalline sponge method an interesting approach to elucidate the structure of such molecules. Unfortunately, their size clearly exceeds the limit imposed by the size of the pores in the metal-organic frameworks based on tris(4-pyridyl)-1,3,5-triazine (TPT). Therefore, the aim of this work was the development of new ligands to be coordinated to Zn(II) salts, substituting longer sidearms with a terminal pyridine moiety for the plain pyridyl group in TPT. As these sidearms need to be rigid in order for the metal-organic framework to form, the plan was to insert ethynyl and 1,4-phenylene bridges between the central aromatic ring and the pyri-

dine. Due to the fact that it is still not sufficiently known whether the central ring needs to be a rather electron-deficient triazine, potential ligands (*cf.* Figure 3.1) include ones with a plain benzene ring at the centre as these compounds are more readily accessible. Ligands **1** and **2** have their sidearms extended only by an ethynyl spacer compared to TPT, whereas ligands **3** and **4** have their sidearms extended by a 1,4-diethynylphenylene bridge.

After successful synthesis of the ligands, the next planned step was to reproduce the synthesis of an adapted version of the original crystalline sponges with $ZnCl_2$ as the metal salt [26] and then adapt the reaction scheme for use of the newly synthesised extended ligands.

4. Results and discussion

4.1. Ligand synthesis

Synthesis of 4',4",4"'-(1,3,5-benzenetriyltri-2,1-ethynediyl)tris-pyridine (**1**) was successful using 1,3,5-trisethynylbenzene and 4-iodopyridine (*cf.* section 5.2.9). The same reaction using 4-bromopyridine hydrochloride as the halide in the Sonogashira coupling did not lead to desired yields. However, this cannot be a general problem of the leaving group, as the direct coupling reaction of 4-bromopyridine hydrochloride with unprotected 1,4-diethynylbenzene in course of the sidearm synthesis for 4',4",4"'-[1,3,5-benzenetriyl-tris(2,1-ethynediyl-4,1-phenylene-2,1-ethynediyl)]tris-pyridine (**3**) worked so well that only the unwanted double substituted product (*cf.* section 5.2.5) was obtained.
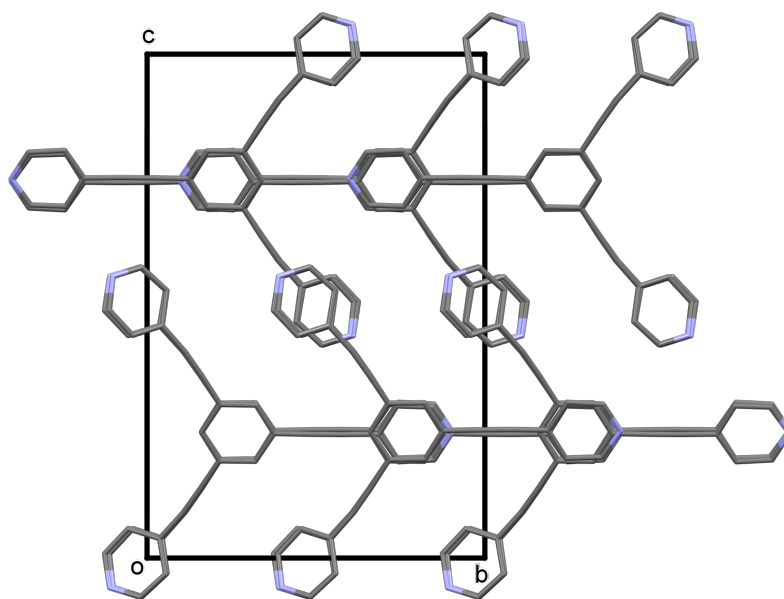
Figure 4.1.: Packing view of ligand **1** along the [100] direction (C: grey; N: blue; hydrogens omitted for clarity)

Although ligand **1** is a compound already known to the literature, its crystal structure was analysed as no structure had been published previously. Single-crystal X-ray diffraction showed π-π-stacking between the central benzene rings (*cf.* Figure 4.1). One of the terminal pyridine rings (N1) is almost exactly parallel to the central ring (bent by 1.83(8) °), while the other two are are strongly bent compared to the benzene (N2: 43.31(8) °; N3: 36.61(8) °, *cf.* Figure 4.2).
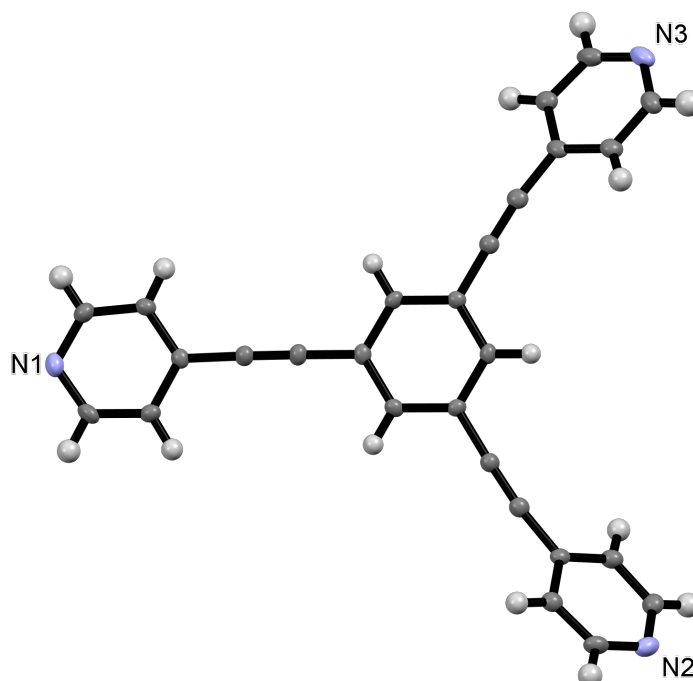
Figure 4.2.: Structural view of ligand **1**, showing 50 % thermal ellipsoids (H: white, other colours: *cf.* Figure 4.1)

Due to these properties, the molecules are ordered in a layered structure in the crystals of ligand **1** (*cf.* Figure 4.3).

In order to obtain 4-[2-(4-ethynylphenyl)ethynyl]-pyridine, protection of one of the two ethynyl groups and deprotection after the coupling reaction was required. Slow addition of stoichiometric amounts of *n*-buthyllithium to a solution of 1,4-diethynylbenzene at -80 °C with subsequent addition of chlorotrimethylsilane gave the single-protected intermediate in acceptable yields (*cf.* section 5.2.6). Interestingly, adding the pyridine moiety to the
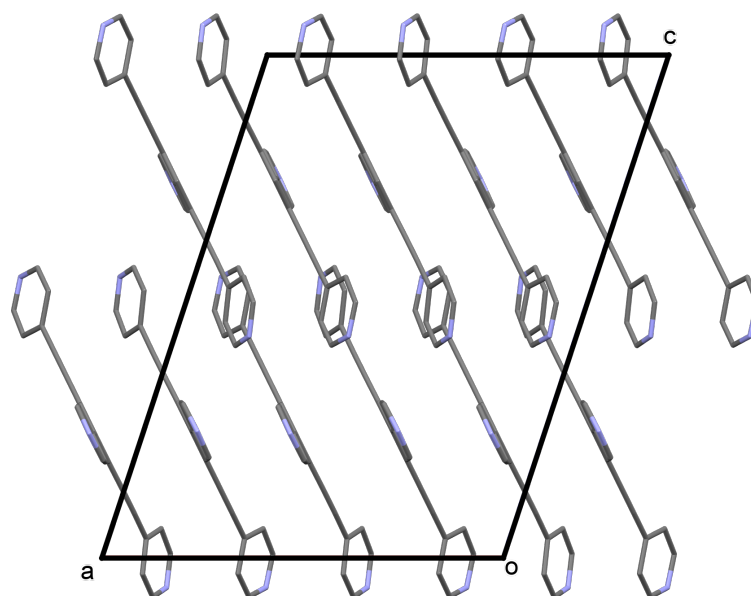
Figure 4.3.: Packing view of ligand **1** along the [010] direction (hydrogens omitted for clarity)

protected sidearm again required 4-iodopyridine as the halide (*cf.* section 5.2.7) because the Sonogashira coupling would lead to yields of less than ten percent when using 4-bromopyridine hydrochloride.

The coupling reaction of 4-[2-(4-ethynylphenyl)ethynyl]-pyridine with 1,3,5-triiodobenzene to give ligand **3** also worked well in the first trial, but due to the small amount of starting material used, X-ray diffraction measurements were not possible although NMR confirmed existence of the product.

Synthesis of ligands **2** and **4** was not completed in the course of this work. The problem with the former was that only small amounts of 4-ethynylpyridine could be obtained via 2-methyl-4-(4-pyridinyl)-3-butyn-2-ol (*cf.* sections 5.2.1 and 5.2.2) and Sonogashira couplings with cyanuric chloride perform poorly. Synthesis of **4** was attempted, but also only with small amounts of starting material. NMR of the raw product did not unambiguously show the desired ligand and the amount of impurities was clearly visible.

Generally speaking, Sonogashira coupling reactions worked well, both with diethylamine and trimethylamine as base. Addition of THF can be helpful in some cases to dissolve the starting material, but the reactions do work in pure base as solvent at least in some cases. Whereever possible, bis(triphenylphosphine)palladium(II) chloride was chosen as a catalyst since it is cheaper than tetrakis(triphenylphosphine)palladium(0) and does not require storage in a glove box.

4.2. MOF synthesis
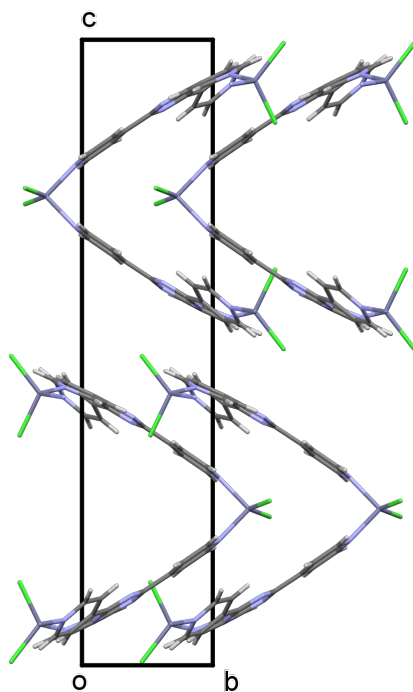
Figure 4.4.: Structural view along the [100] direction of the TPT-based MOF (Cl: green, H: white, Zn: violet, other colours: *cf.* Figure 4.1)

In the beginning, synthesis of crystalline sponge crystals with the original ligand was tried using an adapted procedure (*cf.* section 5.3.1) to learn the technique. The one-dimensional coordination polymer produced was built up of V-shaped chains (*cf.* Figure 4.4). It crystallised in space group $P2/n$. A search of the CCDC database revealed that the

crystal structure of the Iodide analogue is already established [49]. However, Martí-Rujas *et al.* identified the space group as $P2_1$ using synchrotron X-ray powder diffraction. The structures of the TPT-MOF and the analogue (identified in the Cambridge structural database as LUDWEM02, [49]) show high similarity, but are subtly different. It is especially noteworthy that the monoclinic axis in the MOF synthesised in this work is parallel to the channels in the structure, whereas in the analogue, it is perpendicular to the layers.
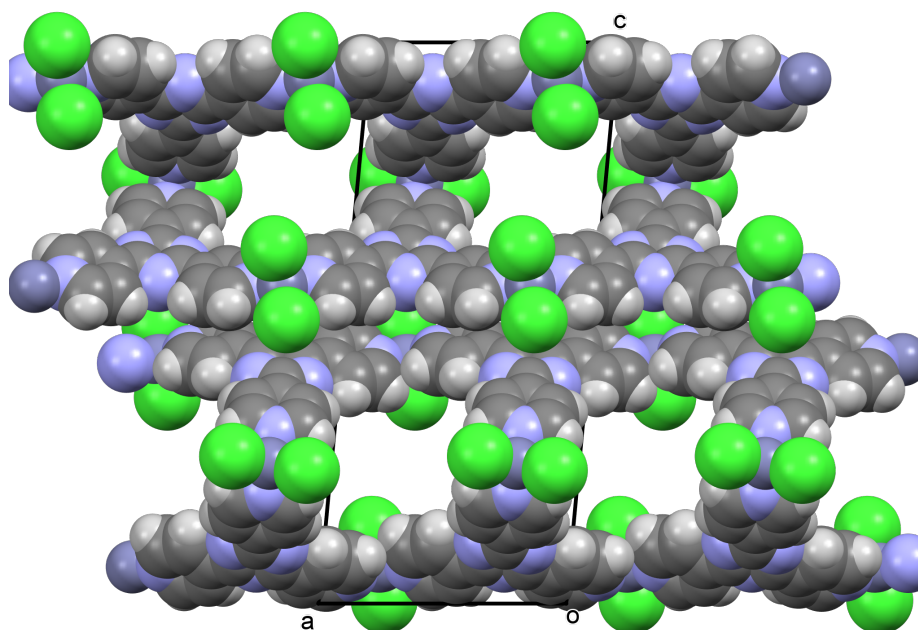
Figure 4.5.: Spacefill model of the crystal structure of the TPT-based MOF, view along the [010] direction, showing pores within the network

Despite the results obtained, Ramadhar *et al.* [26] showed that the system is also able to form two-dimensional coordination polymers, viz. $\{[(\text{ZnCl}_2)_3\text{TPT}_2] \cdot x\,(\text{solvent})\}_n$ does form a two-dimensional coordination network. Due to the lack of time that made the execution of soaking experiments impossible, the question whether the one-dimensional network can act as a proper crystalline sponge is still unresolved. In any case, the crystal structure features solvent-filled pores, which could potentially be occupied by guest molecules (*cf* Figure 4.5). Generally speaking, the reproducibilty of the MOF syntheses is rather poor and Kawano *et al.* [50] have shown that multiple (meta)stable phases depending on the
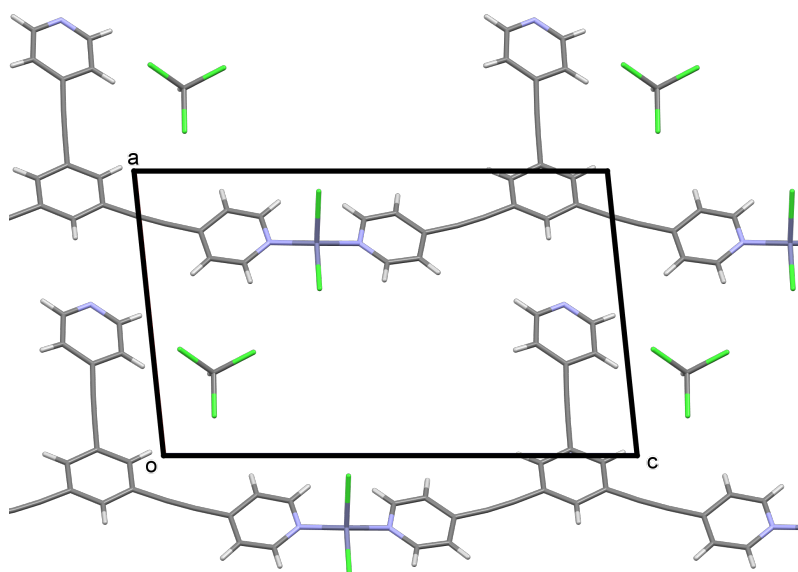
Figure 4.6.: Structural view along the [010] direction of the BTETP-based MOF with encapsulated chloroform molecules

used Zn salt exist. The different phases form depending on reaction time, temperature and possibly other parameters. Interconversion of the metastable double interpenetrating phase formed from TPT and ZnI_2 by crystal growth under kinetic control to the thermodynamic product which is analogous to the MOF based on $ZnCl_2$ described in this work is possible by heating of the crystals [50].
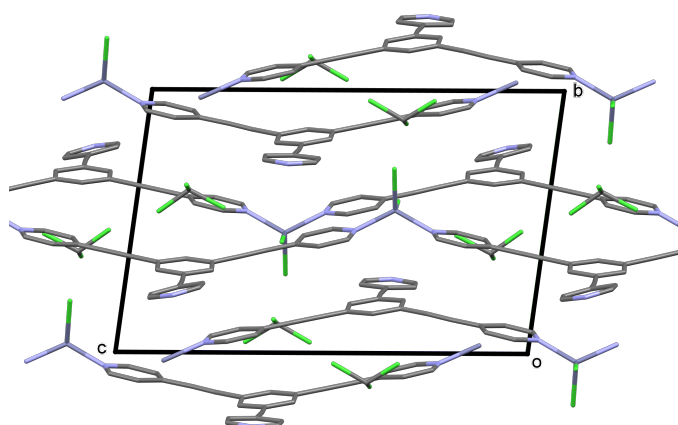
Figure 4.7.: Structural view of the BTETP-based MOF, view along the [100] direction

The synthesis of a metal-organic framework with the ligand 4',4",4'''-[1,3,5-benzenetri-yltris(2,1-ethynediyl-4,1-phenylene-2,1-ethy-nediyl])tris-pyridine (BTETP) and $ZnCl_2$ also led to a one-dimensional polymer structure, but due to denser packing and opposed to the TPT-based MOF, the chloroform molecules encapsulated in the structure were not disordered (*cf.* Figure 4.6 and Figure 4.7). The structure of the resulting MOF was layered. The layers are related by pseudo-symmetry, which leads to an ambiguity in the layer stacking. Stacking faults in the structure lead to systematic twinning (*cf.* Figure 4.8).

Potential usability of this MOF as a crystalline sponge was not evaluated due to time constraints, so soaking experiments and X-ray diffraction experiments of possible inclusion compounds need to be done in a future project.
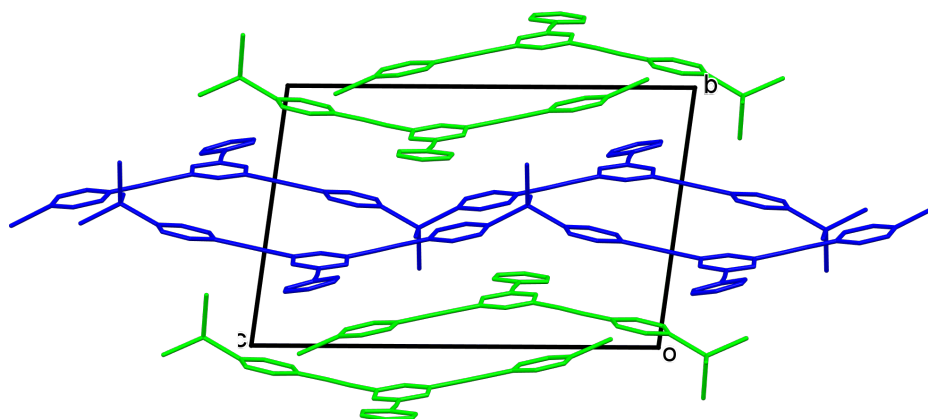
Figure 4.8.: Structural view of the BTETP-based MOF, view along the [100] direction; molecules coloured according to symmetry equivalents (chloroform molecules omitted for clarity)

5. Experimental

5.1. General methodology

The glassware for all reactions carried out under Ar atmosphere was oven-dried at 125 °C for at least two hours before use. The chemicals used were puchased from TCI, Sigma Aldrich or Apollo Scientific and used without further purification. Very sensitive starting materials were stored in a glove box under dry Ar atmosphere and were weighed into dry and argon purged glassware therein.

Infrared spectra were recorded using the ATR technique using a Perkin-Elmer Spectrum Two FTIR spectrometer with an attached UATR accessory. Background measurements were carried out with the anvil opened against ambient air.

NMR spectra were recorded on a Bruker Avance UltraShield 400 MHz spectrometer. Chemical shifts for ^{1}H and ^{13}C are established based on residual solvent resonance and reported in ppm.

5.2. Syntheses

5.2.1. 2-Methyl-4-(4-pyridinyl)-3-butyn-2-ol [51]
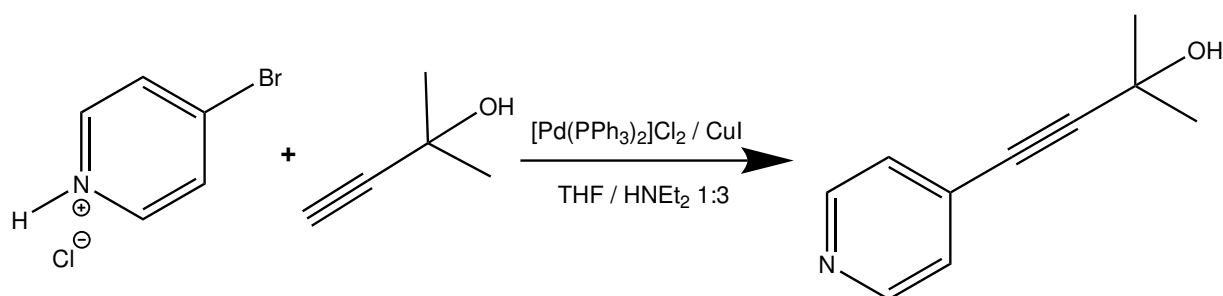
A mixture of 2.55 g (13.1 mmol) 4-bromopyridine hydrochloride, 24.5 mg (129 µmol) CuI and 88 mg (125 µmol) [Pd(PPh$_3$)$_2$]Cl$_2$ was pump-purged with Ar three times and sus-

pended in a mixture of 8 ml absolute THF and 24 ml absolute diethylamine. Then, 1.50 g (17.8 mmol) 2-methyl-3-butyn-2-ol were added. The yellow mixture was stirred at room temperature over night. After completion of the reaction (indicated by TLC, chloroform/EE 1:1), the volatiles were removed *in vacuo*. The remaining solid was taken up in 20 ml of DCM and the solution was washed with saturated NH_4Cl ($2{\times}10$ ml) and water ($2{\times}10$ ml). The organic phase was dried over $MgSO_4$. Removal of the solvent *in vacuo* yielded 2.38 g (113%) of raw product (yellow solid), which was used without further purification.

NMR data:

^{1}H (δ, $CDCl_3$): 8.55 (2H, d, $J = 6.03$ Hz), 7.27 (2H, d, $J = 6.02$ Hz), 3.69 (1H, br s), 1.60 (6H, s)

5.2.2. 4-Ethynylpyridine [51]
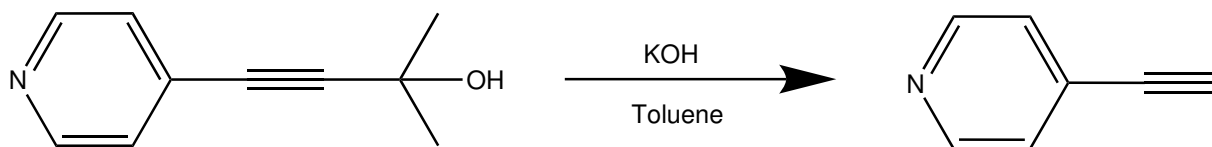
1,30 g (23 mmol) of finely powdered KOH were suspended in a solution of 3.18 g (19.7 mmol) 2-methyl-4-(4-pyridinyl)-3-butyn-2-ol in 90 ml of toluene. The mixture was refluxed for two hours, when TLC (chloroform/EE 1:1) indicated complete consumption of the starting material. When the solution had cooled to room temperature, it was filtered and the solvent was removed *in vacuo*, yielding 1.92 g (94 %) of red crystals as raw product. Sublimation of the raw product (3 mbar, 80 °C) gave 0.41 g (20 %) of 4-Ethynylpyridine as colourless needles.

NMR data:

^{1}H (δ, CD_2Cl_2): 8.57 (2H, d, $J = 6.04$ Hz), 7.35 (2H, d, $J = 6.02$ Hz), 3.36 (1H, s)

5.2.3. 4,4'-(1,4-phenylene)bis[2-methyl-3-butyn-2-ol] [52]
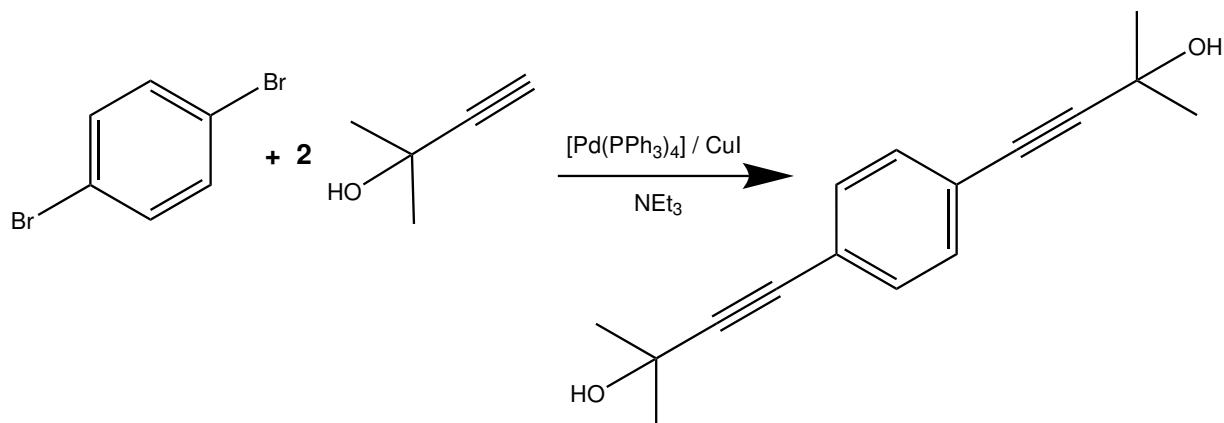
A mixture of 500 mg (2.1 mmol) 1,4-dibromobenzene, 150 mg (0.13 mmol) $[Pd(PPh_3)_4]$ and 40 mg (0.21 mmol) CuI was pump-purged with Ar three times. Then, 15 ml of absolute triethylamine were added. After addition of 600 mg (7.1 mmol) of 2-methyl-3-butyn-2-ol, the mixture was refluxed over night. TLC (PE/EE 1:1) showed complete consumption of 1,4-dibromobenzene. The solvent was removed *in vacuo* and the remaining solid was purified by flash chromatography (silica, PE/EE 1:1), yielding 310 mg (60 %) of the product as off-white crystalline solid.

NMR data:
^{1}H (δ, CDCl$_3$): 7.34 (4H, s), 2.02 (2H, s), 1.61 (12H, s)

5.2.4. 1,4-Diethynylbenzene [52]
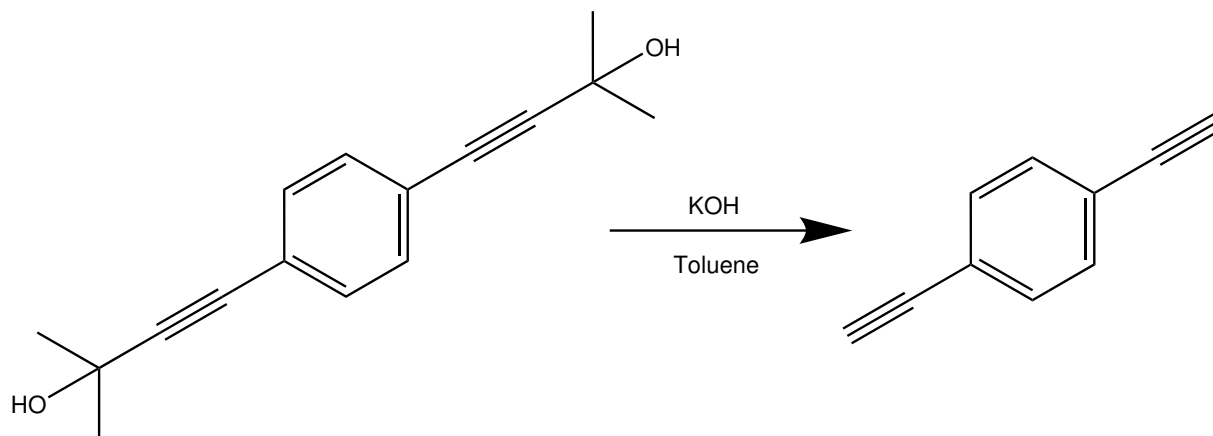
300 mg (1.2 mmol) of 4,4'-(1,4-phenylene)bis[2-methyl-3-butyn-2-ol] were dissolved in 20 ml of toluene and treated with 160 mg (2.9 mmol) of finely powdered KOH. The mixture was refluxed for four hours, when TLC (pure PE) showed completeness of the reaction. Removal of the solvent *in vacuo* and flash chromatography (silica, PE) gave 122 mg (78 %) of the product as colourless crystalline solid.

NMR data:
^{1}H (δ, CDCl$_3$): 7.44 (4H, s), 3.17 (2H, s)
IR data:
ν_{max}/cm^{-1} 3259, 2105, 1920, 1674, 1508, 1494, 1253, 833

5.2.5. 4,4'-(1,4-Phenylenedi-2,1-ethynediyl)bis-pyridine
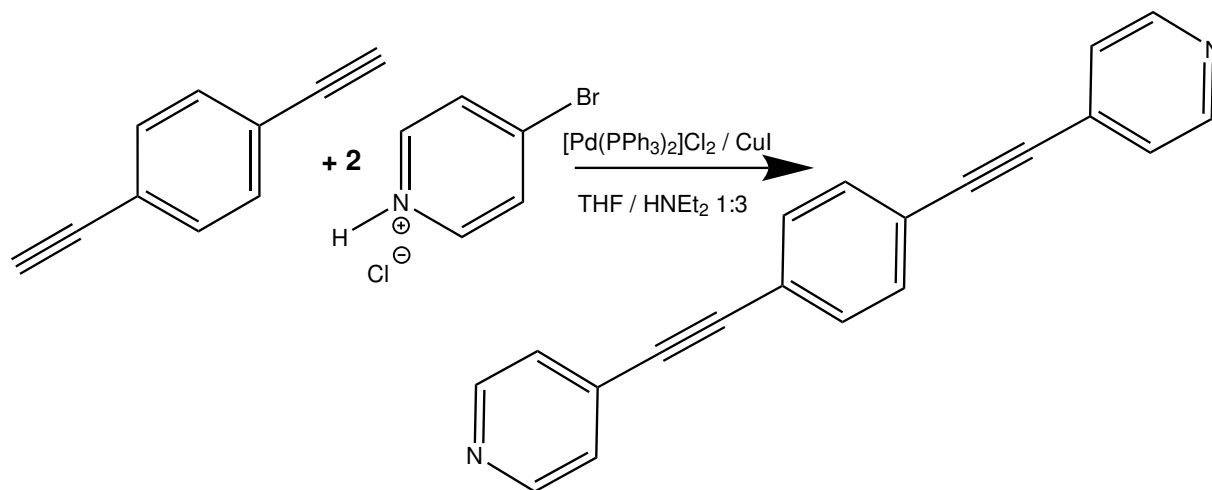
To a mixture of 110 mg (0.57 mmol) 4-bromopyridine hydrochloride, 290 mg (2.3 mmol) 1,4-diethynylbenzene, 8 mg (42 µmol) CuI and 13 mg (19 µmol) $[Pd(PPh_3)_2]Cl_2$ under Ar was added 10 ml absolute THF and 30 ml of absolute diethylamine. The solution was stirred at room temperature over night. TLC (DCM/*n*-hexane 1:1) showed completeness of the reaction. The volatiles were removed *in vacuo*. The raw product was purified by column chromatography (DCM/MeOH 19:1), giving the product as off-white solid in 60 % yield (95 mg).

NMR data:

^{1}H (δ, CD_2Cl_2): 8.60 (4H, d, $J = 5.32$ Hz, 7.59 (4H, s), 7.40 (4H, d, $J = 6.06$ Hz)

5.2.6. 1-Ethynyl-4-[2-(trimethylsilyl)ethynyl]-benzene [53]
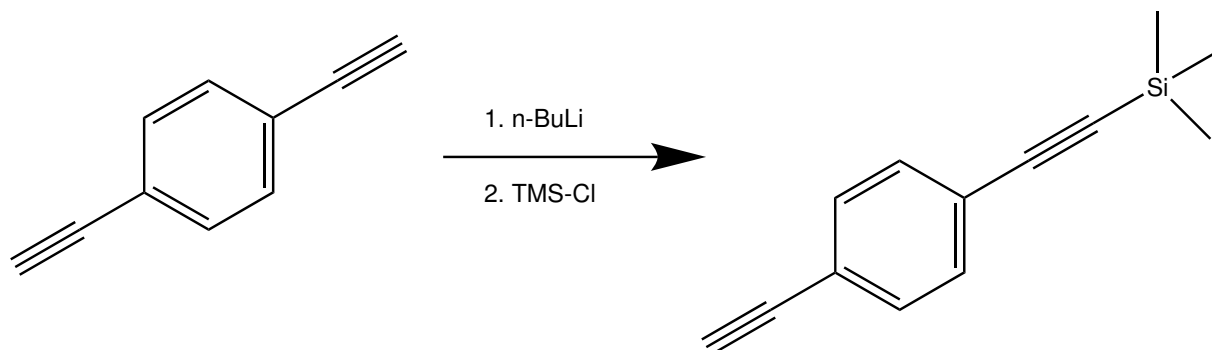
A solution of 499 mg (4.0 mmol) 1,4-diethynylbenzene in 50 ml in absolute THF under Ar was cooled to -78 °C. Then, 1.8 ml of a 2.5 M solution of *n*-BuLi in hexane was added over one hour. After stirring for two hours at -78 °C, 0.69 g (6.4 mmol) of chlorotrimethylsilane were added and the solution was stirred over night, allowing it to slowly reach room temperature. The solvent was removed *in vacuo* whereat the colour changed from pale yellow to intense orange. The remainders were dissolved in 20 ml of ether and washed with 20 ml of water. The organic phase was dried over $MgSO_4$ and the solvent removed *in vacuo*, giving 548 mg (70 %) of the product as red oil, which was used without further purification.

NMR data:

^{1}H (δ, $CDCl_3$): 7.41 (4H, s), 3.16 (1H, s), 0.25 (9H, s)

^{13}C{^{1}H} (δ, $CDCl_3$): 132.06, 131.97, 123.73, 122.25, 104.49, 96.61, 83.35, 79.09, 0.04

IR data:

ν_{max}/cm^{-1} 3263, 2962, 2157, 1497, 1251, 836

5.2.7. 4-[2-[4-[2-(trimethylsilyl)ethynyl]phenyl]ethynyl]-pyridine
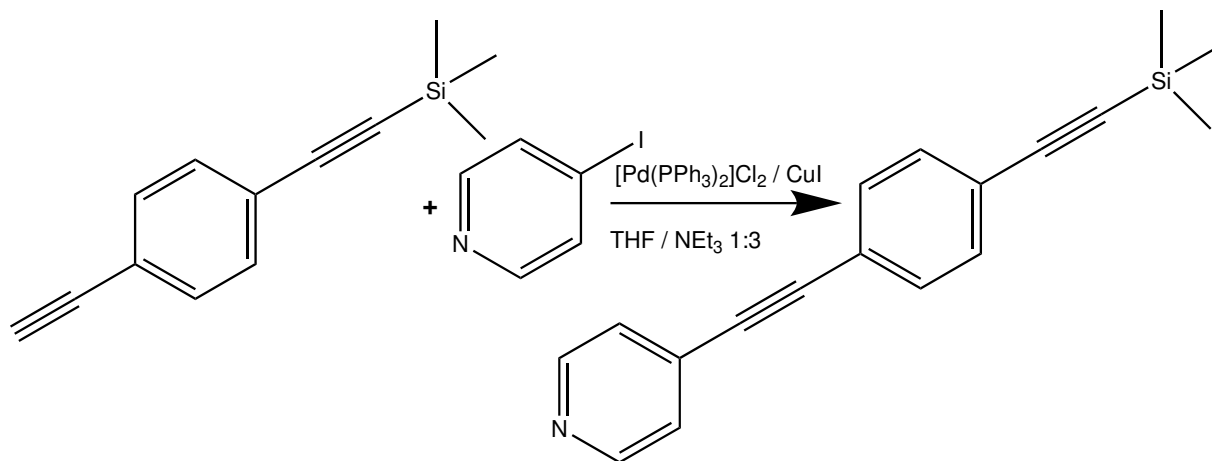
A mixture of 295 mg (1.5 mmol) 1-ethynyl-4-[2-(trimethylsilyl)ethynyl]-benzene, 296 mg (1.4 mmol) 4-iodopyridine, 15 mg (79 µmol) CuI and 52 mg (74 µmol) [Pd(PPh$_3$)$_2$]Cl$_2$ under Ar was dissolved in 8 ml of absolute THF. After addition of 24 ml of absolute triethylamine, the solution was stirred at 50 °C over night. After TLC (DCM/MeOH 19:1) indicated completion of the reaction, the volatiles were removed. The raw product was subjected to column chromatography (silica, DCM/MeOH 19:1) and 279 mg (70 %) of the product were isolated as off-white solid.

^{1}H (δ, CDCl$_3$): 8.69 (2H, d, $J = 5.81$ Hz), 7.43 (2H, d, $J = 4.77$ Hz), 7.39 (4H, s), 0.24 (9H, s)

5.2.8. 4-[2-(4-Ethynylphenyl)ethynyl]-pyridine
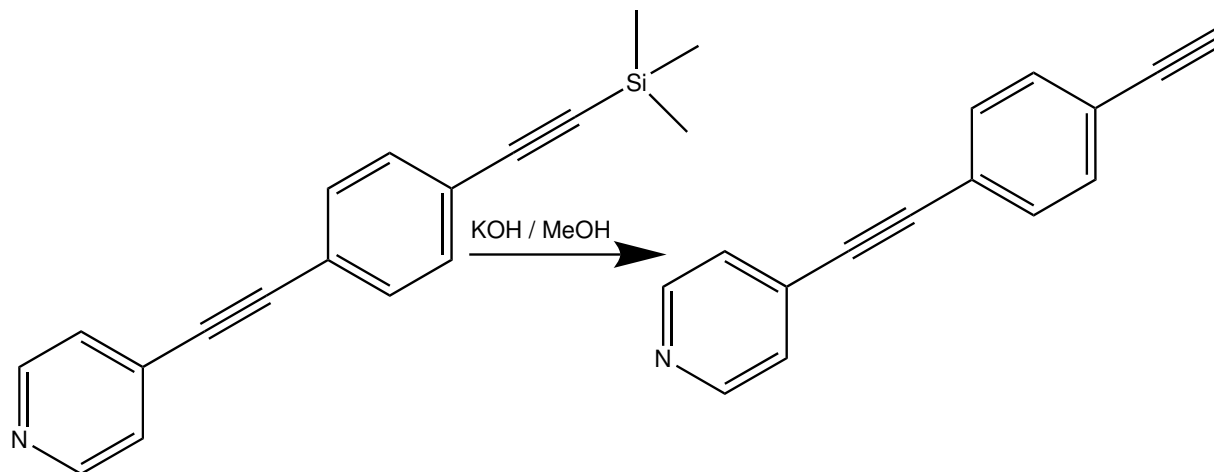
265 mg (962 µmol) of 4-[2-[4-[2-(trimethylsilyl)ethynyl]phenyl]ethynyl]-pyridine were dissolved in 30 ml of MeOH. 1.1 ml of 1M KOH were added and the mixture was stirred at room temperature and the reaction monitored by TLC (DCM/MeOH 19:1). After stirring over night, 15 ml of 1M NH_4Cl were added to the solution. The reaction mixture was extracted four times with 10 ml of DCM and the combined organic phases were dried over $MgSO_4$ and the solvent removed *in vacuo*. Column chromatography (silica, DCM/MeOH 19:1) gave the product as pale yellow solid (170 mg, 87%).

NMR data:

^{1}H (δ, CDCl$_3$): 8.61 (2H, d, $J = 6.11$ Hz), 7.50 (4H, s), 7.38 (2H, d, $J = 6.05$ Hz), 3.20 (1H, s)

5.2.9. 4',4'',4'''-(1,3,5-Benzenetriyltri-2,1-ethynediyl)tris-pyridine (BTETP)
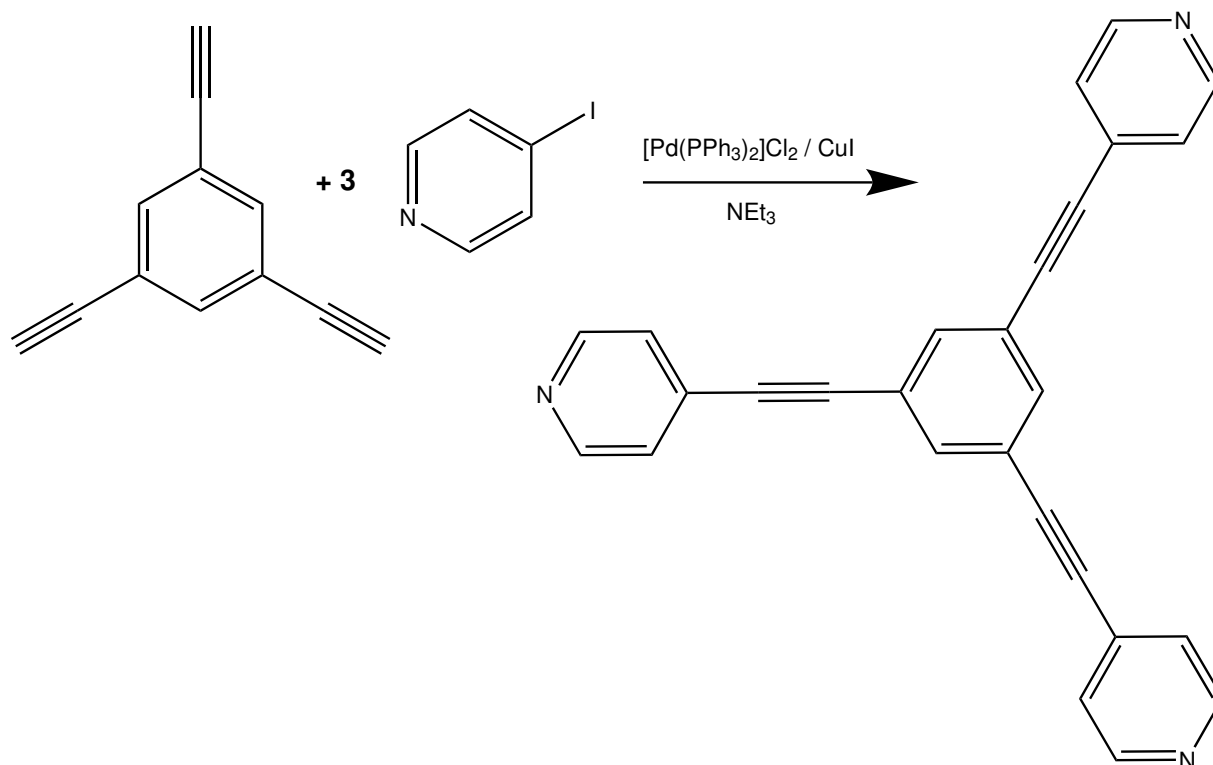
A synthetic procedure adapted from Lee *et al.* [54] and Ecija *et al.* [55] was used.

A mixture of 100 mg (0.7 mmol) 1,3,5-triethynylbenzene, 540 mg (2.6 mmol) 4-iodo-pyridine, 7.6 mg (40 μmol) CuI and 21.0 mg (30 μmol) [Pd(PPh$_3$)$_2$]Cl$_2$ under Ar was dissolved in 24 ml of absolute triethylamine. The solution was refluxed over night. TLC (EE/MeOH 5:1) indicated complete consumption of 1,3,5-triethynylbenzene. The solvent was removed *in vacuo* and the remainders redissolved in 50 ml of EE.

This solution was then filtered to remove brown insoluble solids and the filtrate was washed with saturated NH$_4$Cl (2×20 ml) and water (2×20 ml). The organic phase was dried over MgSO$_4$ and evaporated *in vacuo*. Column chromatography of the raw product (silica, EE/MeOH 5:1) gave 178 mg (70 %) of the product as pale yellow solid.

A small amount of the product was later re-dissolved in DCM, filtered through a syringe filter and put in a glass vial equipped with a screw cap with a septum. The septum was pierced with a needle to allow slow evaporation of the solvent. The crystals obtained were subjected to X-ray diffraction analysis.

NMR data:

^{1}H (δ, CDCl$_3$): 8.65 (6, d, $J = 6.08$ Hz), 7.75 (3H, s), 7.39 (6H, d, $J = 6.05$ Hz)

^{13}C\{^{1}H\} (δ, CDCl$_3$): 150.10, 135.35, 130.76, 125.67, 123.53, 91.58, 88.40

IR data:

ν_{max}/cm^{-1} 3036, 2216, 1592, 1407, 1216, 990, 882, 816

5.2.10. 4',4'',4'''-[1,3,5-Benzenetriyltris(2,1-ethynediyl-4,1-phenylene-2,1-ethynediyl)]tris-pyridine
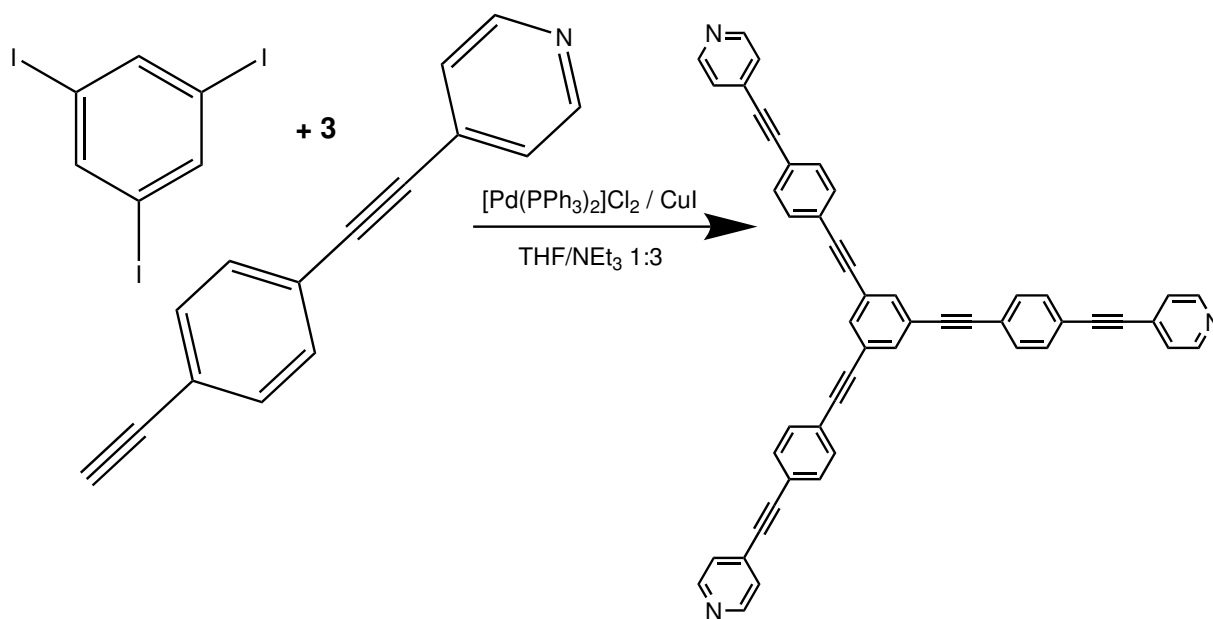
A mixture of 23.5 mg (116 μmol) 4-[2-(4-ethynylphenyl)ethynyl]-pyridine, 13.7 mg (30 μmol), 1 mg (5.3 μmol) CuI and 2 mg (2.9 μmol) [Pd(PPh$_3$)$_2$]Cl$_2$ under Ar was dissolved in 1 ml of

absolute THF. After addition of 3 ml of absolute triethylamine, the solution was heated to 55 °C and stirred over night, when TLC (DCM/MeOH 19:1) indicated completion of the reaction.

After removal of the volatiles *in vacuo*, the remainders were redissolved in 10 ml of DCM and filtered. The solution was washed with saturated NH_4Cl (1 ml) and water (2 ml), dried over $MgSO_4$ and evaporated, yielding 19.5 mg (95 %) of raw product. Due to the small amount, no further purification was applied, but the NMR data was in accordance with the literature [56]

NMR data:

^{1}H (δ, $CDCl_3$): 8.61 (6 H, d, $J = 6.08$ Hz), 7.67 (3 H, s), 7.54 (12 H, s), 7.38 (6 H, d, $J = 6.10$ Hz)

^{13}C{^{1}H} (δ, $CDCl_3$): 149.93, 134.45, 131.85, 129.00, 125.61, 123.97, 123.62, 122.43, 93.48, 90.33, 90.05, 88.72

IR data:

ν_{max}/cm^{-1} 2922, 2216, 1588, 1509, 1405, 1102, 988, 817

5.3. Crystal growth

5.3.1. TPT-based MOF

This procedure was adapted from the original publication by Inokuma *et al.* [28]. ZnI_2 was replaced by $ZnCl_2$ and the solvent system chloroform/MeOH was used as described by Ramadhar *et al.* [27].

In multiple glass vials, 0.5 ml of a solution of tris-(4-pyridinyl)-1,3,5-triazine (TPT) in chloroform (c = 1.3 mg·ml^{-1}) were carefully overlayed with the same amount of pure chloroform and pure MeOH. Then, 0.5 ml of a methanolic solution of anhydrous $ZnCl_2$ (c = 10 mg·ml^{-1}) were added carefully in order to avoid immediate mixing of the two phases. The vials were capped with a septum and stored at room temperature for 7 days. After a

few hours, an opaque phase appeared at the interface and after a few days, larger crystals started to grow.

5.3.2. BTETP-based MOF

The procedure for growing MOF crystals with 4',4'',4'''-(1,3,5-benzenetriyltri-2,1-ethynedi-yl)tris-pyridine as the ligand was the same as described in section 5.3.1, but the concentrations of $ZnCl_2$ and the ligand were adapted to $5.5\,mg{\cdot}ml^{-1}$ and $4.7\,mg{\cdot}ml^{-1}$, respectively.

5.4. X-ray diffraction measurements

Intensity data of BTETP, the TPT-based MOF and the BTETP-based MOF were collected at $100\,K$ in a dry stream of nitrogen on a Bruker KAPPA APEX II diffractometer system[1] using graphite monochromatized $Mo\,K_{\overline{\alpha}}$ radiation in fine-sliced ω- and φ-scans.

Whereas the data collection and reduction of BTETP and the TPT-based MOF were routine, the BTETP-based MOF featured splitting reflections, a common sign of twinning.

Therefore, numerous crystals of said MOF were probed in short scans and the crystal with the best compromise between intensity and mosaicity was selected. A full sphere of reciprocal space was collected with increased detector distance to resolve close reflections. Two domains were then identified using the RLATT module[1]. They were concurrently integrated with overlap information (HKLF5-style format) using SAINT-Plus[1].

A correction for absorption effects was performed using the multi-scan approach implemented in SADABS (BTETP, TPT-based MOF) or TWINABS (BTETP-based MOF)[1]. The structures were solved with the dual-space approach implemented in SHELX [57] and refined against F^2 with SHELXT [58].

In case of the crystal structure of the TPT-based MOF, contributions of disordered solvent molecules to the structure factors were removed using the SQUEEZE routine of PLATON [59]. Table 5.1 shows crystal data, data collection information and refinement

---

[1]Bruker Analytical X-ray Instruments, Inc., Madison, WI, USA.
 APEXII, RLATT, SAINT, SADABS and TWINABS, 2017.

data for the measured crystals. For atomic coordinates, displacement and geometric parameters, see Appendix A.

Table 5.1.: Crystal data details of the refinements for the measured crystals

	Ligand	TPT-based MOF	BTETP-based MOF
Crystal data			
Chemical formula	$C_{27}H_{15}N_3$	$C_{18}H_{12}Cl_3N_6Zn_{1.5}$	$C_{28}H_{16}Cl_5N_3Zn$
M_r	381.42	516.74	637.06
Cell setting, space group	Monoclinic, $C2/c$	Monoclinic, $P2/n$	Triclinic, $P\overline{1}$
Temperature (K)	100	100	100
a, b, c (Å)	15.539 (3), 13.068 (3), 20.498 (4)	12.9824 (13), 6.1372 (7), 29.497 (3)	12.4371 (19), 13.286 (2), 18.397 (3)
$\alpha(°)$	90	90	95.607 (5)
$\beta(°)$	108.197 (9)	95.334 (3)	92.733 (5)
$\gamma(°)$	90	90	117.035 (4)
V (Å^3)	3954.4 (14)	2340.0 (4)	2680.1 (7)
Z	8	4	4
D_x (Mg m^{-3})	1.281	1.467	1.579
Radiation type	Mo K$_{\overline{\alpha}}$	Mo K$_{\overline{\alpha}}$	Mo K$_{\overline{\alpha}}$
μ(mm^{-1})	0.08	1.91	1.44
Crystal form, colour	block, colourless	block, colourless	plate, colourless
Crystal size (mm)	$0.32 \times 0.28 \times 0.04$	$0.12 \times 0.06 \times 0.02$	$0.53 \times 0.42 \times 0.11$
Data collection			
Diffractometer	Bruker KAPPA APEX II CCD	Bruker KAPPA APEX II CCD	Bruker KAPPA APEX II CCD
Data collection method	ω- and φ-scans	ω- and φ-scans	ω- and φ-scans
Absorption correction	multi-scan SADABS	multi-scan SADABS	multi-scan SADABS
$T_{\min}$, $T_{\max}$	0.697, 0.746	0.432, 0.492	0.539, 0.746
No. of measured, independent and observed reflections	41603, 4667, 2854	16026, 6054, 4600	43039, 11964, 9796

Table continued on the next page

Table 5.1.: Crystal data details of the refinements for the measured crystals (cont.)

	Ligand	TPT-based MOF	BTETP-based MOF
Criterion for observed reflections	$I > 2\sigma(I)$	$I > 2\sigma(I)$	$I > 2\sigma(I)$
R_{int}	0.065	0.040	0.078
$\theta_{\min}$, $\theta_{\max}$ (°)	2.1, 27.9	2.7, 28.9	1.1, 28.3
Refinement			
Refinement on	F^2	F^2	F^2
$R[F^2 > 2\sigma(F^2)]$, $wR(F^2)$, S	0.048, 0.149, 1.01	0.039, 0.096, 1.02	0.057, 0.143, 1.07
No. of reflections	4667	6051	11964
No. of parameters	271	258	668
Constraints	0	0	0
Primary atom site location	SHELXT	SHELXT	SHELXT
Secondary atom site location	Difference Fourier	Difference Fourier	Difference Fourier
Weighting scheme	$1/[\sigma^2(F_o{}^2 + (0.0842P)^2 + 0.3473P]$ where $P = (F_o{}^2 + 2F_c{}^2)/3$	$1/[\sigma^2(F_o{}^2 + (0.0474P)^2]$ where $P = (F_o{}^2 + 2F_c{}^2)/3$	$1/[\sigma^2(F_o{}^2 + (0.0361P)^2 + 12.2623P]$ where $P = (F_o{}^2 + 2F_c{}^2)/3$
$(\Delta/\sigma)_{\max}$	0.001	0.003	0.001
$\Delta\rho_{\max}$, $\Delta\rho_{\min}$ (e Å^3)	0.41, -0.23	0.59, -0.36	1.06, -0.84
Extinction correction	none	none	none
Extinction coefficient	-	-	-

6. Conclusion

Two potential ligands for use in crystalline sponges with extended void volumes were successfully synthesised. The smaller of the two benzene-centred candidate ligands was successfully characterised using single-crystal X-ray diffraction. Synthesis of the two candidate ligands with a closer relation to the originally used TPT ligands, bearing a 1,3,5-triazine centre could not be finished as the Sonogashira coupling reactions with cyanuric chloride as the halide compound were unsuccessful and time constraints prevented the development of a better protocol. Synthesis of these compounds can, however, very likely be completed in a subsequent work.

Synthesis of metal-organic frameworks with $ZnCl_2$ and the ligands tris-(4-pyridinyl)-1,3,5-triazine and 4',4'',4'''-(1,3,5-benzenetriyltri-2,1-ethynediyl)tris-pyridine was tried out and the product crystals examined with X-ray diffraction, showing that one-dimensional coordination polymers had formed. The crystals obtained were not tested for their guest inclusion ability, and further investigations will be necessary.

Further studies of the MOF-forming protocols and their improvement will be required to obtain two or three-dimensional coordination networks, in case the one-dimensional structures are not sufficient.

Generally speaking, the crystalline sponge method requires a lot of experience and development of protocols fitting the users' needs is very labour-intensive. Cooperation with an experienced crystallographer is clearly beneficial.

Bibliography

[1] "Chemistry"., *Dictionary.com Unabridged*, Dictionary.com, LLC, `http : / / www . dictionary.com/browse/chemistry` (retrieved on 2017-07-10).

[2] "Chemistry"., *Merriam-Webster.com*, Merriam-Webster, `https : / / www . merriam - webster.com/dictionary/chemistry` (retrieved on 2017-07-10).

[3] Bagley, M. What Is Chemistry?, `https://www.livescience.com/45986-what-is-chemistry.html` (retrieved on 2017-07-10).

[4] Inokuma, Y.; Yoshioka, S.; Ariyoshi, J.; Arai, T.; Hitora, Y.; Takada, K.; Matsunaga, S.; Rissanen, K.; Fujita, M. *Nature*, **2013**, *495*, 461–466, DOI: `10.1038/nature11990`.

[5] Vinogradova, E. V.; Müller, P.; Buchwald, S. L. *Angew. Chem., Int. Ed.* **2014**, *53*(12), 3125–3128, DOI: `10.1002/anie.201310897`.

[6] Müller, D. Main Group (IV) element substituted tetrazoles for iron(II) spin crossover compounds., Master's thesis, Technische Universität Wien, 2012.

[7] Müller, D.; Knoll, C.; Stöger, B.; Artner, W.; Reissner, M.; Weinberger, P. *Eur. J. Inorg. Chem.* **2013**, *2013*(5), 984–991, DOI: `10.1002/ejic.201201062`.

[8] Seifried, M.; Knoll, C.; Giester, G.; Reissner, M.; Müller, D.; Weinberger, P. *Magnetochemistry*, **2016**, *2*(1), 12, DOI: `10.3390/magnetochemistry2010012`.

[9] Müller, D.; Knoll, C.; Seifried, M.; Weinberger, P. *Vib. Spectrosc.* **2016**, *86*, 198–205, DOI: `10.1016/j.vibspec.2016.06.011`.

[10] Seifried, M.; Knoll, C.; Giester, G.; Welch, J. M.; Müller, D.; Weinberger, P. *Eur. J. Org. Chem.* **2017**, *2017*(17), 2416–2424, DOI: `10.1002/ejoc.201700105`.

[11] Hoshino, M.; Khutia, A.; Xing, H.; Fujita, M.; Inokuma, Y. *IUCrJ*, **2016**, *3*(2), 139–151, DOI: `10.1107/S2052252515024379`.

[12] Stallforth, P.; Clardy, J. *Nature,* **2013**, *495,* 456–457, DOI: 10.1038/495456a.

[13] Inokuma, Y.; Yoshioka, S.; Ariyoshi, J.; Arai, T.; Hitora, Y.; Takada, K.; Matsunaga, S.; Rissanen, K.; Fujita, M. *Nature,* **2013**, *501,* 262, DOI: 10.1038/nature12527.

[14] Fujita, M.; Oguro, D.; Miyazawa, M.; Oka, H.; Yamaguchi, K.; Ogura, K. *Nature,* **1995**, *378,* 469–471, DOI: 10.1038/378469a0.

[15] Inokuma, Y.; Arai, T.; Fujita, M. *Nat. Chem.* **2010**, *2*(9), 780–783, DOI: 10.1038/nchem.742.

[16] Biradha, K.; Fujita, M. *Angew. Chem., Int. Ed.* **2002**, *41*(18), 3392–3395, DOI: 10.1002/1521-3773(20020916)41:18<3392::AID-ANIE3392>3.0.CO;2-V.

[17] Abrahams, B. F.; Batten, S. R.; Hamit, H.; Hoskins, B. F.; Robson, R. *Angew. Chem., Int. Ed.* **1996**, *35*(15), 1690–1692, DOI: 10.1002/anie.199616901.

[18] Ohmori, O.; Kawano, M.; Fujita, M. *J. Am. Chem. Soc.* **2004**, *126*(50), 16292–16293, DOI: 10.1021/ja046478a.

[19] Ohmori, O.; Kawano, M.; Fujita, M. *Angew. Chem., Int. Ed.* **2005**, *44*(13), 1962–1964, DOI: 10.1002/anie.200462201.

[20] Csöregh, I.; Czugler, M.; Weber, E.; Ahrendt, J. *J. Inclusion Phenom. Mol. Recognit. Chem.* **1990**, *8*(3), 309–322, DOI: 10.1007/BF01041887.

[21] Byrn, M. P.; Curtis, C. J.; Hsiou, Y.; Khan, S. I.; Sawin, P. A.; Tendick, S. K.; Terzis, A.; Strouse, C. E. *J. Am. Chem. Soc.* **1993**, *115*(21), 9480–9497, DOI: 10.1021/ja00074a013.

[22] Pang, L.; Lucken, E. A.; Bernardinelli, G. *J. Inclusion Phenom. Macrocyclic Chem.* **1992**, *13*(1), 63–76.

[23] Gangu, K. K.; Maddila, S.; Mukkamala, S. B.; Jonnalagadda, S. B. *Inorg. Chim. Acta,* **2016**, *446,* 61 –74, DOI: 10.1016/j.ica.2016.02.062.

[24] Callaway, E. *Nat. News,* **2013**, DOI: 10.1038/nature.2013.13798.

[25] Halford, B. *Chem. Eng. News*, **2013**, *91*(38), `http://cen.acs.org/articles/91/i38/Crystal-Free-Crystallization-Loses-Lustre.html` (retrieved on 2017-07-14).

[26] Ramadhar, T. R.; Zheng, S.-L.; Chen, Y.-S.; Clardy, J. *Chem. Commun.* **2015**, *51*(56), 11252–11255, DOI: `10.1039/C5CC03840E`.

[27] Ramadhar, T. R.; Zheng, S.-L.; Chen, Y.-S.; Clardy, J. *Acta Crystallogr., Sect. A: Found. Adv.* **2015**, *71*(1), 46–58, DOI: `10.1107/S2053273314019573`.

[28] Inokuma, Y.; Yoshioka, S.; Ariyoshi, J.; Arai, T.; Fujita, M. *Nat. Protoc.* **2014**, *9*(2), 246–252, DOI: `10.1038/nprot.2014.007`.

[29] Matsuda, Y.; Mitsuhashi, T.; Lee, S.; Hoshino, M.; Mori, T.; Okada, M.; Zhang, H.; Hayashi, F.; Fujita, M.; Abe, I. *Angew. Chem.* **2016**, *128*(19), 5879–5882, DOI: `10.1002/ange.201601448`.

[30] Brkljača, R.; Schneider, B.; Hidalgo, W.; Otálvaro, F.; Ospina, F.; Lee, S.; Hoshino, M.; Fujita, M.; Urban, S. *Molecules*, **2017**, *22*(2), 211, DOI: `10.3390/molecules22020211`.

[31] Lee, S.; Hoshino, M.; Fujita, M.; Urban, S. *Chem. Sci.* **2017**, *8*(2), 1547–1550, DOI: `10.1039/C6SC04288K`.

[32] Urban, S.; Brkljača, R.; Hoshino, M.; Lee, S.; Fujita, M. *Angewandte Chemie*, **2016**, *128*(8), 2728–2732, DOI: `10.1002/ange.201509761`.

[33] Inokuma, Y.; Fujita, M. *Bull. Chem. Soc. Jpn.* **2014**, *87*(11), 1161–1176, DOI: `10.1246/bcsj.20140217`.

[34] Peplow, M. *ACS Cent. Sci.* **2016**, *2*(5), 268–269, DOI: `10.1021/acscentsci.6b00136`.

[35] Yoshioka, S.; Inokuma, Y.; Hoshino, M.; Sato, T.; Fujita, M. *Chem. Sci.* **2015**, *6*(7), 3765–3768, DOI: `10.1039/C5SC01681A`.

[36] Ikemoto, K.; Inokuma, Y.; Rissanen, K.; Fujita, M. *J. Am. Chem. Soc.* **2014**, *136* (19), 6892–6895, DOI: 10.1021/ja502996h.

[37] Sanna, E.; Escudero-Adán, E. C.; Bauzá, A.; Ballester, P.; Frontera, A.; Rotger, C.; Costa, A. *Chem. Sci.* **2015**, *6* (10), 5466–5472, DOI: 10.1039/C5SC01838B.

[38] Zhang, S.-Y.; Wojtas, L.; Zaworotko, M. J. *J. Am. Chem. Soc.* **2015**, *137* (37), 12045–12049, DOI: 10.1021/jacs.5b06760.

[39] Waldhart, G. W.; Mankad, N. P.; Santarsiero, B. D. *Org. Lett.* **2016**, *18* (23), 6112–6115, DOI: 10.1021/acs.orglett.6b03119.

[40] Brunet, G.; Safin, D. A.; Korobkov, I.; Cognigni, A.; Murugesu, M. *Cryst. Growth Des.* **2016**, *16* (7), 4043–4050, DOI: 10.1021/acs.cgd.6b00570.

[41] Gu, X.-F.; Zhao, Y.; Li, K.; Su, M.-X.; Yan, F.; Li, B.; Du, Y.-X.; Di, B. *J. Chromatogr. A*, **2016**, *1474*, 130–137, DOI: 10.1016/j.chroma.2016.10.072.

[42] Lee, S.; Kapustin, E. A.; Yaghi, O. M. *Science*, **2016**, *353*, 808–811, DOI: 10.1126/science.aaf9135.

[43] Qin, J.-S.; Yuan, S.; Alsalme, A.; Zhou, H.-C. *ACS Appl. Mater. Interfaces*, **2017**, DOI: 10.1021/acsami.6b16264.

[44] Hayes, L. M.; Knapp, C. E.; Nathoo, K. Y.; Press, N. J.; Tocher, D. A.; Carmalt, C. J. *Cryst. Growth Des.* **2016**, *16* (6), 3465–3472, DOI: 10.1021/acs.cgd.6b00435.

[45] Hayes, L. M.; Press, N. J.; Tocher, D. A.; Carmalt, C. J. *Cryst. Growth Des.* **2017**, *17* (2), 858–863, DOI: 10.1021/acs.cgd.6b01694.

[46] Duplan, V.; Hoshino, M.; Li, W.; Honda, T.; Fujita, M. *Angew. Chem., Int. Ed.* **2016**, *55* (16), 4919–4923, DOI: 10.1002/anie.201509801.

[47] Cuenca, A. B.; Zigon, N.; Duplan, V.; Hoshino, M.; Fujita, M.; Fernández, E. *Chem. - Eur. J.* **2016**, *22* (14), 4723–4726, DOI: 10.1002/chem.201600392.

[48] Brunet, G.; Safin, D. A.; Jover, J.; Ruiz, E.; Murugesu, M. *J. Mater. Chem. C*, **2017**, *5* (4), 835–841, DOI: 10.1039/C6TC04703C.

[49] Martí-Rujas, J.; Islam, N.; Hashizume, D.; Izumi, F.; Fujita, M.; Kawano, M. *J. Am. Chem. Soc.* **2011**, *133*(15), 5853–5860, DOI: `10.1021/ja109160a`.

[50] Kawano, M.; Haneda, T.; Hashizume, D.; Izumi, F.; Fujita, M. *Angew. Chem., Int. Ed.* **2008**, *47*(7), 1269–1271, DOI: `10.1002/anie.200704809`.

[51] Yu, L.; Lindsey, J. S. *J. Org. Chem.* **2001**, *66*(22), 7402–7419, DOI: `10.1021/jo010742q`.

[52] Shu, W.; Guan, C.; Guo, W.; Wang, C.; Shen, Y. *J. Mater. Chem.* **2012**, *22*(7), 3075–3081, DOI: `10.1039/c1jm15535k`.

[53] Liu, Y.; Jiang, S.; Glusac, K.; Powell, D. H.; Anderson, D. F.; Schanze, K. S. *J. Am. Chem. Soc.* **2002**, *124*(42), 12412–12413, DOI: `10.1021/ja027639i`.

[54] Lee, S. J.; Mulfort, K. L.; O'Donnell, J. L.; Zuo, X.; Goshe, A. J.; Wesson, P. J.; Nguyen, S. T.; Hupp, J. T.; Tiede, D. M. *Chem. Commun.* **2006**, (44), 4581–4583, DOI: `10.1039/b610025b`.

[55] Ecija, D.; Vijayaraghavan, S.; Auwärter, W.; Joshi, S.; Seufert, K.; Aurisicchio, C.; Bonifazi, D.; Barth, J. V. *ACS Nano*, **2012**, *6*(5), 4258–4265, DOI: `10.1021/nn3007948`.

[56] Kelley, R. F.; Lee, S. J.; Wilson, T. M.; Nakamura, Y.; Tiede, D. M.; Osuka, A.; Hupp, J. T.; Wasielewski, M. R. *J. Am. Chem. Soc.* **2008**, *130*(13), 4277–4284, DOI: `10.1021/ja075494f`.

[57] Sheldrick, G. M. *Acta Crystallogr., Sect. A: Found. Adv.* **2015**, *71*(1), 3–8, DOI: `10.1107/S2053273314026370`.

[58] Sheldrick, G. M. *Acta Crystallogr., Sect. C: Struct. Chem.* **2015**, *71*(1), 3–8, DOI: `10.1107/S2053229614024218`.

[59] Spek, A. L. *Acta Crystallogr., Sect. C: Struct. Chem.* **2015**, *71*(1), 9–18, DOI: `10.1107/S2053229614024929`.

A. Crystallographic data

Table A.1.: Fractional atomic coordinates and isotropic or equivalent isotropic displacement parameters (Å^2) of BTETP

	x	y	z	U_{iso}*/U_{eq}
N1	0.63312 (9)	0.09835 (10)	0.74756 (7)	0.0275 (3)
C1	0.62063 (10)	0.62413 (11)	0.74715 (8)	0.0182 (3)
N2	0.93258 (9)	1.10079 (11)	1.05869 (7)	0.0286 (3)
C2	0.67793 (10)	0.67682 (11)	0.80353 (7)	0.0180 (3)
H2	0.716413	0.639693	0.841267	0.022*
N3	0.31490 (9)	1.11029 (11)	0.44127 (8)	0.0320 (4)
C3	0.67881 (10)	0.78349 (11)	0.80460 (7)	0.0167 (3)
C4	0.62232 (10)	0.83854 (11)	0.74926 (7)	0.0176 (3)
H4	0.623319	0.911224	0.749879	0.021*
C5	0.56425 (10)	0.78651 (11)	0.69290 (7)	0.0168 (3)
C9	0.62490 (10)	0.31295 (11)	0.74595 (7)	0.0177 (3)
C8	0.62214 (10)	0.42265 (12)	0.74517 (8)	0.0211 (4)
C7	0.62107 (10)	0.51432 (12)	0.74567 (8)	0.0208 (3)
C6	0.56352 (10)	0.67957 (11)	0.69208 (7)	0.0176 (3)
H6	0.524010	0.644251	0.653894	0.021*
C10	0.57046 (10)	0.25557 (12)	0.69112 (8)	0.0212 (4)
H10	0.529624	0.288107	0.652255	0.025*
C11	0.57750 (11)	0.15026 (12)	0.69485 (8)	0.0247 (4)
H11	0.540156	0.111862	0.657276	0.030*
C12	0.68428 (11)	0.15490 (12)	0.79960 (8)	0.0239 (4)
H12	0.724422	0.119993	0.837693	0.029*
C13	0.68291 (10)	0.26047 (12)	0.80191 (8)	0.0205 (4)
H13	0.720468	0.296539	0.840597	0.025*
C14	0.73799 (10)	0.83838 (11)	0.86209 (8)	0.0195 (3)
C15	0.78614 (11)	0.88725 (12)	0.90894 (8)	0.0208 (4)
C16	0.83942 (10)	0.95541 (11)	0.96090 (8)	0.0183 (3)
C17	0.85176 (10)	0.94119 (12)	1.03062 (8)	0.0227 (4)
H17	0.828917	0.881776	1.046250	0.027*
C18	0.89788 (11)	1.01515 (13)	1.07672 (8)	0.0257 (4)
H18	0.905452	1.004657	1.124048	0.031*
C19	0.92248 (11)	1.11193 (13)	0.99200 (8)	0.0267 (4)
H19	0.947771	1.171040	0.978084	0.032*

Table A.1.: Fractional atomic coordinates and isotropic or equivalent isotropic displacement parameters (Å^2) of BTETP (cont.)

	x	y	z	$U_{\text{iso}}*/U_{\text{eq}}$
C20	0.87750 (10)	1.04277 (12)	0.94192 (8)	0.0233 (4)
H20	0.872567	1.054558	0.895157	0.028*
C21	0.50504 (10)	0.84352 (12)	0.63654 (8)	0.0201 (3)
C22	0.45695 (10)	0.89324 (12)	0.58997 (8)	0.0214 (4)
C23	0.40537 (10)	0.96273 (12)	0.53864 (8)	0.0210 (4)
C24	0.37641 (11)	1.05560 (12)	0.55837 (9)	0.0253 (4)
H24	0.386753	1.070428	0.605571	0.030*
C25	0.33269 (11)	1.12553 (13)	0.50869 (9)	0.0308 (4)
H25	0.314055	1.188412	0.523275	0.037*
C26	0.34137 (11)	1.02037 (13)	0.42253 (9)	0.0297 (4)
H26	0.328908	1.007501	0.374861	0.036*
C27	0.38578 (10)	0.94487 (13)	0.46827 (8)	0.0245 (4)
H27	0.402554	0.882226	0.452071	0.029*

Table A.2.: Atomic displacement parameters (Å^2) of BTETP

	U^{11}	U^{22}	U^{33}	U^{12}	U^{13}	U^{23}
N1	0.0287 (8)	0.0182 (7)	0.0351 (8)	−0.0006 (6)	0.0093 (7)	0.0025 (6)
C1	0.0211 (8)	0.0167 (8)	0.0198 (8)	0.0006 (6)	0.0108 (6)	−0.0006 (6)
N2	0.0237 (8)	0.0325 (8)	0.0261 (8)	0.0004 (6)	0.0025 (6)	−0.0075 (6)
C2	0.0200 (8)	0.0198 (8)	0.0149 (8)	0.0031 (6)	0.0063 (6)	0.0012 (6)
N3	0.0231 (8)	0.0336 (9)	0.0341 (9)	−0.0022 (6)	0.0012 (7)	0.0140 (7)
C3	0.0170 (8)	0.0191 (8)	0.0145 (8)	−0.0006 (6)	0.0057 (6)	−0.0024 (6)
C4	0.0208 (8)	0.0149 (7)	0.0193 (8)	−0.0005 (6)	0.0094 (6)	−0.0015 (6)
C5	0.0174 (8)	0.0189 (8)	0.0150 (7)	0.0007 (6)	0.0062 (6)	0.0000 (6)
C9	0.0192 (8)	0.0177 (8)	0.0187 (8)	0.0008 (6)	0.0093 (6)	0.0015 (6)
C8	0.0244 (8)	0.0193 (8)	0.0198 (8)	−0.0007 (7)	0.0072 (7)	−0.0002 (6)
C7	0.0249 (8)	0.0180 (8)	0.0209 (8)	−0.0009 (6)	0.0093 (7)	−0.0010 (6)
C6	0.0195 (8)	0.0184 (8)	0.0153 (7)	−0.0023 (6)	0.0063 (6)	−0.0047 (6)
C10	0.0205 (8)	0.0229 (9)	0.0180 (8)	0.0012 (6)	0.0024 (7)	0.0017 (6)
C11	0.0262 (9)	0.0228 (9)	0.0226 (9)	−0.0039 (7)	0.0042 (7)	−0.0036 (7)
C12	0.0229 (9)	0.0248 (9)	0.0228 (9)	0.0040 (7)	0.0054 (7)	0.0095 (7)
C13	0.0206 (8)	0.0235 (9)	0.0166 (8)	−0.0027 (7)	0.0045 (7)	−0.0006 (6)
C14	0.0213 (8)	0.0195 (8)	0.0179 (8)	0.0015 (6)	0.0064 (6)	0.0001 (6)
C15	0.0222 (8)	0.0220 (9)	0.0191 (8)	0.0019 (7)	0.0077 (7)	0.0003 (6)

Table continued on the next page

Table A.2.: Atomic displacement parameters (Å^2) of BTETP (cont.)

	U^{11}	U^{22}	U^{33}	U^{12}	U^{13}	U^{23}
C16	0.0154 (7)	0.0219 (8)	0.0164 (8)	0.0029 (6)	0.0033 (6)	−0.0010 (6)
C17	0.0215 (8)	0.0248 (9)	0.0216 (8)	0.0024 (7)	0.0066 (7)	0.0012 (7)
C18	0.0248 (9)	0.0343 (10)	0.0163 (8)	0.0036 (7)	0.0039 (7)	−0.0019 (7)
C19	0.0232 (9)	0.0252 (9)	0.0295 (9)	−0.0015 (7)	0.0050 (7)	−0.0002 (7)
C20	0.0215 (8)	0.0279 (9)	0.0194 (8)	0.0005 (7)	0.0047 (7)	0.0016 (7)
C21	0.0201 (8)	0.0211 (8)	0.0192 (8)	−0.0005 (6)	0.0065 (7)	0.0004 (7)
C22	0.0194 (8)	0.0246 (9)	0.0214 (8)	−0.0011 (7)	0.0078 (7)	0.0010 (7)
C23	0.0154 (8)	0.0251 (9)	0.0215 (8)	−0.0013 (6)	0.0043 (6)	0.0046 (7)
C24	0.0200 (8)	0.0287 (9)	0.0251 (9)	0.0022 (7)	0.0040 (7)	0.0013 (7)
C25	0.0239 (9)	0.0266 (10)	0.0380 (11)	0.0018 (7)	0.0038 (8)	0.0059 (8)
C26	0.0242 (9)	0.0386 (11)	0.0224 (9)	−0.0076 (8)	0.0015 (7)	0.0080 (8)
C27	0.0215 (9)	0.0271 (9)	0.0238 (9)	−0.0039 (7)	0.0057 (7)	0.0028 (7)

Table A.3.: Geometric parameters (Å, °) of BTETP

N1–C12	1.337 (2)	C6–C5–C21	120.46 (14)	C25–H25	0.9500
N1–C11	1.338 (2)	C4–C5–C21	119.78 (13)	C26–C27	1.387 (2)
C1–C2	1.400 (2)	C10–C9–C13	118.08 (14)	C26–H26	0.9500
C1–C6	1.400 (2)	C10–C9–C8	121.30 (14)	C27–H27	0.9500
C1–C7	1.435 (2)	C13–C9–C8	120.61 (14)	C12–C13–H13	120.8
N2–C19	1.334 (2)	C7–C8–C9	178.77 (19)	C9–C13–H13	120.8
N2–C18	1.343 (2)	C8–C7–C1	179.3 (2)	C15–C14–C3	177.75 (17)
C2–C3	1.394 (2)	C5–C6–C1	120.46 (14)	C14–C15–C16	173.80 (16)
C2–H2	0.9500	C5–C6–H6	119.8	C17–C16–C20	117.41 (14)
N3–C25	1.337 (2)	C1–C6–H6	119.8	C17–C16–C15	122.73 (14)
N3–C26	1.340 (2)	C11–C10–C9	118.26 (14)	C20–C16–C15	119.79 (14)
C3–C4	1.397 (2)	C11–C10–H10	120.9	C18–C17–C16	118.87 (15)
C3–C14	1.439 (2)	C9–C10–H10	120.9	C18–C17–H17	120.6
C4–C5	1.3999 (19)	N1–C11–C10	124.74 (15)	C16–C17–H17	120.6
C4–H4	0.9500	N1–C11–H11	117.6	N2–C18–C17	124.09 (15)
C5–C6	1.398 (2)	C10–C11–H11	117.6	N2–C18–H18	118.0
C5–C21	1.440 (2)	N1–C12–C13	124.61 (14)	C17–C18–H18	118.0
C9–C10	1.395 (2)	N1–C12–H12	117.7	N2–C19–C20	124.05 (16)
C9–C13	1.397 (2)	C13–C12–H12	117.7	N2–C19–H19	118.0
C9–C8	1.434 (2)	C12–C13–C9	118.37 (14)	C20–C19–H19	118.0
C8–C7	1.198 (2)	C11–H11	0.9500	C19–C20–C16	119.19 (15)
C6–H6	0.9500	C12–C13	1.381 (2)	C19–C20–H20	120.4

Table continued on the next page

Table A.3.: Geometric parameters (Å, °) of BTETP (cont.)

C10–C11	1.381 (2)	C12–H12	0.9500	C16–C20–H20	120.4
C10–H10	0.9500	C13–H13	0.9500	C22–C21–C5	178.37 (17)
C12–N1–C11	115.93 (14)	C14–C15	1.201 (2)	C21–C22–C23	173.25 (17)
C2–C1–C6	119.37 (13)	C15–C16	1.436 (2)	C24–C23–C27	117.24 (14)
C2–C1–C7	120.21 (14)	C16–C17	1.394 (2)	C24–C23–C22	119.70 (14)
C6–C1–C7	120.42 (14)	C16–C20	1.396 (2)	C27–C23–C22	122.98 (14)
C19–N2–C18	116.35 (14)	C17–C18	1.385 (2)	C25–C24–C23	119.39 (16)
C3–C2–C1	120.36 (13)	C17–H17	0.9500	C25–C24–H24	120.3
C3–C2–H2	119.8	C18–H18	0.9500	C23–C24–H24	120.3
C1–C2–H2	119.8	C19–C20	1.382 (2)	N3–C25–C24	124.04 (16)
C25–N3–C26	116.36 (14)	C19–H19	0.9500	N3–C25–H25	118.0
C2–C3–C4	120.09 (13)	C20–H20	0.9500	C24–C25–H25	118.0
C2–C3–C14	120.78 (14)	C21–C22	1.203 (2)	N3–C26–C27	124.22 (16)
C4–C3–C14	119.13 (13)	C22–C23	1.431 (2)	N3–C26–H26	117.9
C3–C4–C5	119.97 (13)	C23–C24	1.397 (2)	C27–C26–H26	117.9
C3–C4–H4	120.0	C23–C27	1.398 (2)	C26–C27–C23	118.73 (16)
C5–C4–H4	120.0	C24–C25	1.379 (2)	C26–C27–H27	120.6
C6–C5–C4	119.75 (13)	C24–H24	0.9500	C23–C27–H27	120.6

Table A.4.: Fractional atomic coordinates and isotropic or equivalent isotropic displacement parameters (Å^2) of the TPT-based MOF

	x	y	z	$U_{\mathrm{iso}}*/U_{\mathrm{eq}}$
Zn1	0.26484 (2)	1.32176 (5)	0.56538 (2)	0.01932 (9)
Cl1	0.23574 (5)	1.54120 (10)	0.50560 (2)	0.02411 (15)
C1	0.67973 (18)	0.8007 (4)	0.58128 (8)	0.0165 (5)
N1	0.67610 (15)	0.6116 (3)	0.60342 (7)	0.0161 (4)
Zn2	0.7500	–0.27689 (7)	0.7500	0.02615 (12)
Cl2	0.31235 (6)	1.47645 (13)	0.63229 (2)	0.03606 (18)
C2	0.85369 (18)	0.8030 (4)	0.58837 (8)	0.0168 (5)
N2	0.76595 (14)	0.9034 (3)	0.57231 (7)	0.0164 (4)
C3	0.76809 (18)	0.5271 (4)	0.61840 (8)	0.0163 (5)
N3	0.85940 (14)	0.6168 (3)	0.61171 (7)	0.0163 (4)
Cl3	0.59807 (6)	–0.43477 (12)	0.73725 (3)	0.03948 (19)
C4	0.57911 (18)	0.9107 (4)	0.56911 (8)	0.0173 (5)
N4	0.39065 (15)	1.1286 (3)	0.55602 (8)	0.0221 (5)
C5	0.48848 (19)	0.8145 (4)	0.58088 (9)	0.0236 (6)
H5	0.4900	0.6727	0.5938	0.028*

Table continued on the next page

Table A.4.: Fractional atomic coordinates and isotropic or equivalent isotropic displacement parameters (Å²) of the TPT-based MOF (cont.)

	x	y	z	$U_{\text{iso}}*/U_{\text{eq}}$
N5	1.13501 (15)	1.1391 (3)	0.57169 (8)	0.0204 (5)
N6	0.76126 (17)	–0.0445 (3)	0.69954 (7)	0.0218 (5)
C6	0.39635 (19)	0.9262 (4)	0.57360 (10)	0.0258 (6)
H6	0.3346	0.8579	0.5813	0.031*
C9	0.95236 (18)	0.9164 (4)	0.58146 (8)	0.0182 (5)
C8	0.57284 (18)	1.1157 (4)	0.54886 (8)	0.0170 (5)
H8	0.6327	1.1834	0.5391	0.020*
C7	0.47788 (18)	1.2193 (4)	0.54323 (9)	0.0199 (5)
H7	0.4740	621280	0.5298	0.024*
C10	0.95391 (19)	1.0921 (4)	0.55219 (9)	0.0208 (5)
H10	0.8922	1.1395	0.5352	0.025*
C11	1.04663 (19)	1.1978 (4)	0.54794 (9)	0.0219 (5)
H11	1.0475	462399	0.5274	0.026*
C12	1.1325 (2)	0.9727 (5)	0.60127 (10)	0.0282 (6)
H12	16072	0.9348	0.6192	0.034*
C13	1.04409 (19)	0.8549 (4)	0.60666 (10)	0.0260 (6)
H13	1.0455	0.7347	0.6270	0.031*
C14	0.76657 (18)	0.3264 (4)	0.64600 (8)	0.0160 (5)
C15	0.8583 (2)	0.2286 (4)	0.66449 (8)	0.0201 (5)
H15	0.9236	0.2876	0.6589	0.024*
C16	0.8521 (2)	0.0439 (4)	0.69108 (8)	0.0218 (5)
H16	0.9143	–0.0225	0.7038	0.026*
C17	0.6738 (2)	0.0514 (4)	0.68198 (8)	0.0218 (5)
H17	0.6096	–0.0110	0.6882	0.026*
C18	0.6726 (2)	0.2357 (4)	0.65546 (9)	0.0201 (5)
H18	0.6090	0.3000	0.6438	0.024*

Table A.5.: Atomic displacement parameters (Å²) of the TPT-based MOF

	U^{11}	U^{22}	U^{33}	U^{12}	U^{13}	U^{23}
Zn1	0.01452 (15)	0.01661 (14)	0.02683 (18)	–0.00154 (11)	0.00201 (11)	0.00582 (12)
Cl1	0.0232 (3)	0.0233 (3)	0.0257 (3)	–0.0015 (2)	0.0015 (2)	0.0089 (3)
C1	0.0174 (12)	0.0143 (11)	0.0181 (12)	–0.0025 (9)	0.0027 (9)	–0.0024 (9)
N1	0.0172 (10)	0.0126 (9)	0.0184 (11)	–0.0008 (8)	0.0012 (8)	–0.0001 (8)
Zn2	0.0483 (3)	0.0142 (2)	0.0168 (2)	0.000	0.00720 (19)	0.000

Table A.5.: Atomic displacement parameters (Å^2) of TPT-based MOF (cont.)

	U^{11}	U^{22}	U^{33}	U^{12}	U^{13}	U^{23}
Cl2	0.0416 (4)	0.0390 (4)	0.0277 (4)	−0.0153 (3)	0.0036 (3)	0.0014 (3)
C2	0.0200 (12)	0.0123 (11)	0.0185 (12)	0.0007 (9)	0.0045 (9)	−0.0009 (9)
N2	0.0148 (10)	0.0133 (9)	0.0212 (11)	−0.0009 (8)	0.0023 (8)	−0.0010 (8)
C3	0.0195 (12)	0.0145 (11)	0.0149 (12)	−0.0029 (9)	0.0022 (9)	−0.0042 (9)
N3	0.0180 (10)	0.0143 (9)	0.0169 (11)	−0.0005 (8)	0.0028 (8)	−0.0010 (8)
Cl3	0.0603 (5)	0.0251 (4)	0.0342 (4)	−0.0150 (3)	0.0105 (4)	−0.0040 (3)
C4	0.0169 (12)	0.0163 (11)	0.0187 (13)	−0.0038 (10)	0.0012 (10)	−0.0022 (10)
N4	0.0140 (10)	0.0180 (10)	0.0340 (13)	−0.0025 (8)	0.0008 (9)	0.0023 (9)
C5	0.0211 (13)	0.0152 (12)	0.0348 (16)	−0.0033 (10)	0.0046 (11)	0.0048 (11)
N5	0.0144 (10)	0.0186 (10)	0.0285 (12)	0.0005 (8)	0.0036 (9)	0.0057 (9)
N6	0.0355 (13)	0.0152 (10)	0.0152 (11)	−0.0015 (9)	0.0052 (9)	0.0001 (8)
C6	0.0187 (13)	0.0181 (12)	0.0413 (17)	−0.0060 (10)	0.0066 (11)	0.0042 (12)
C9	0.0159 (12)	0.0158 (11)	0.0235 (14)	−0.0015 (10)	0.0048 (10)	−0.0020 (10)
C8	0.0148 (11)	0.0173 (11)	0.0188 (13)	−0.0035 (9)	0.0000 (9)	0.0017 (10)
C7	0.0197 (12)	0.0167 (12)	0.0228 (13)	−0.0035 (10)	−0.0005 (10)	0.0033 (10)
C10	0.0159 (12)	0.0210 (12)	0.0252 (14)	−0.0010 (10)	0.0007 (10)	0.0032 (11)
C11	0.0192 (12)	0.0197 (12)	0.0267 (14)	−0.0012 (10)	0.0019 (10)	0.0063 (11)
C12	0.0171 (13)	0.0292 (15)	0.0380 (17)	−0.0009 (11)	0.0013 (11)	0.0119 (12)
C13	0.0198 (13)	0.0222 (13)	0.0364 (17)	0.0001 (10)	0.0043 (11)	0.0131 (12)
C14	0.0217 (12)	0.0134 (11)	0.0130 (12)	0.0004 (9)	0.0034 (9)	−0.0040 (9)
C15	0.0269 (14)	0.0160 (12)	0.0179 (13)	−0.0003 (10)	0.0044 (10)	−0.0014 (10)
C16	0.0293 (14)	0.0180 (12)	0.0179 (13)	0.0019 (11)	0.0010 (10)	0.0005 (10)
C17	0.0266 (14)	0.0189 (12)	0.0206 (14)	−0.0058 (11)	0.0063 (11)	−0.0004 (10)
C18	0.0240 (13)	0.0181 (12)	0.0187 (13)	−0.0031 (10)	0.0046 (10)	−0.0011 (10)

Table A.6.: Geometric parameters (Å, °) of the TPT-based MOF

Zn1–N5$^{\text{i}}$	2.047 (2)	N2–C2–C9	116.7 (2)	C17—C18	1.375 (3)
Zn1–N4	2.058 (2)	C1–N2–C2	114.5 (2)	C17–H17	0.9500
Zn1–Cl1	2.2230 (7)	N3–C3–N1	124.6 (2)	C18–H18	0.9500
Zn1–Cl2	2.2249 (8)	N3–C3–C14	118.8 (2)	N4–C6–C5	122.4 (2)
C1–N2	1.332 (3)	N1–C3–C14	116.6 (2)	N4–C6–H6	118.8
C1–N1	1.335 (3)	C2–N3–C3	114.9 (2)	C5–C6–H6	118.8
C1–C4	1.484 (3)	C8–C4–C5	118.3 (2)	C10–C9–C13	118.8 (2)
N1–C3	1.339 (3)	C8–C4–C1	122.0 (2)	C10–C9–C2	120.9 (2)
Zn2–N6$^{\text{ii}}$	2.076 (2)	C5–C4–C1	119.5 (2)	C13–C9–C2	120.2 (2)

Table continued on the next page

Table A.6.: Geometric parameters (Å, °) of the TPT-based MOF (cont.)

Zn2–N6	2.077 (2)	C6–N4–C7	118.2 (2)	C7–C8–C4	118.9 (2)
Zn2–Cl3	2.1983 (8)	C6–N4–Zn1	119.75 (17)	C7–C8–H8	120.6
Zn2–Cl3^{ii}	2.1983 (8)	C7–N4–Zn1	119.87 (17)	C4–C8–H8	120.6
C2–N3	1.333 (3)	C6–C5–C4	119.5 (2)	N4–C7–C8	122.7 (2)
C2–N2	1.342 (3)	C6–C5–H5	120.2	N4–C7–H7	118.7
C2–C9	1.488 (3)	C4–C5–H5	120.2	C8–C7–H7	118.7
C3–N3	1.338 (3)	C11–N5–C12	118.2 (2)	C9–C10–C11	119.1 (2)
C3–C14	1.478 (3)	C11–N5–Zn1^{iii}	118.60 (17)	C9–C10–H10	120.5
C4–C8	1.392 (3)	C12–N5–Zn1^{iii}	122.99 (17)	C11–C10–H10	120.5
C4–C5	1.389 (3)	C17–N6–C16	118.6 (2)	N5–C11–C10	122.5 (2)
N4–C6	1.345 (3)	C17–N6–Zn2	117.71 (17)	N5–C11–H11	118.7
N4–C7	1.347 (3)	C16–N6–Zn2	122.16 (17)	C10–C11–H11	118.7
C5–C6	1.378 (4)	N5–C12	1.345 (3)	N5–C12–C13	122.9 (2)
C5–H5	0.9500	N5–Zn1^{iii}	2.047 (2)	N5–C12–H12	118.5
N5–C11	1.337 (3)	N6–C17	1.340 (3)	C13–C12–H12	118.5
N5^{i}–Zn1–N4	111.54 (8)	N6–C16	1.343 (3)	C12–C13–C9	118.4 (2)
N5^{i}–Zn1–Cl1	108.86 (6)	C6–H6	0.9500	C12–C13–H13	120.8
N4–Zn1–Cl1	108.73 (7)	C9–C10	1.382 (3)	C9–C13–H13	120.8
N5^{i}–Zn1–Cl2	108.40 (7)	C9–C13	1.396 (4)	C18–C14–C15	118.7 (2)
N4–Zn1–Cl2	101.94 (7)	C8–C7	1.383 (3)	C18–C14–C3	120.0 (2)
Cl1–Zn1–Cl2	117.24 (3)	C8–H8	0.9500	C15–C14–C3	121.2 (2)
N2–C1–N1	125.2 (2)	C7–H7	0.9500	C16–C15–C14	118.7 (2)
N2–C1–C4	118.3 (2)	C10–C11	1.383 (3)	C16–C15–H15	120.6
N1–C1–C4	116.3 (2)	C10–H10	0.9500	C14–C15–H15	120.6
C1–N1–C3	115.3 (2)	C11–H11	0.9500	N6–C16–C15	122.3 (2)
N6^{ii}–Zn2–N6	93.22 (11)	C12–C13	1.378 (3)	N6–C16–H16	118.9
N6^{ii}–Zn2–Cl3	107.68 (6)	C12–H12	0.9500	C15–C16–H16	118.9
N6–Zn2–Cl3	107.57 (6)	C13–H13	0.9500	N6–C17–C18	123.1 (2)
N6^{ii}–Zn2–Cl3^{ii}	107.57 (6)	C14–C18	1.393 (3)	N6–C17–H17	118.5
N6–Zn2–Cl3^{ii}	107.68 (6)	C14–C15	1.398 (3)	C18–C17–H17	118.5
Cl3–Zn2–Cl3^{ii}	127.70 (5)	C15–C16	1.385 (3)	C17–C18–C14	118.6 (2)
N3–C2–N2	125.5 (2)	C15–H15	0.9500	C17–C18–H18	120.7
N3–C2–C9	117.7 (2)	C16–H16	0.9500	C14–C18–H18	120.7

Table A.7.: Fractional atomic coordinates and isotropic or equivalent isotropic displacement parameters (Å^2) of the BTETP-based MOF

	x	y	z	$U_{\text{iso}}*/U_{\text{eq}}$
Zn1	0.75674 (6)	–0.03083 (6)	–0.12033 (4)	0.01838 (15)
Zn2	0.74617 (6)	0.54398 (6)	0.37004 (4)	0.01858 (15)
Cl1	0.92025 (14)	–0.05642 (15)	–0.12128 (8)	0.0302 (4)
Cl2	0.58108 (13)	–0.19299 (13)	–0.12731 (8)	0.0225 (3)
Cl3	0.92803 (13)	0.70046 (13)	0.38577 (8)	0.0237 (3)
Cl4	0.58693 (14)	0.57807 (14)	0.36602 (9)	0.0274 (3)
Cl5	1.6266 (2)	0.53636 (19)	–0.05752 (11)	0.0506 (5)
Cl6	1.63702 (16)	0.55149 (17)	–0.21233 (9)	0.0383 (4)
Cl7	1.86005 (17)	0.63665 (17)	–0.11558 (10)	0.0387 (4)
Cl8	0.8536 (3)	0.9592 (2)	0.46743 (13)	0.0675 (7)
Cl9	0.63310 (18)	0.87304 (17)	0.37202 (10)	0.0399 (4)
Cl10	0.8649 (2)	0.9588 (2)	0.31167 (13)	0.0585 (6)
N1	0.7573 (4)	0.0532 (4)	–0.0209 (3)	0.0200 (10)
N2	0.7420 (4)	0.0373 (4)	0.7880 (3)	0.0186 (10)
N3	–0.0420 (5)	0.2819 (5)	0.3551 (3)	0.0301 (13)
N4	0.7489 (5)	0.4623 (4)	0.2706 (3)	0.0205 (10)
N5	0.7456 (4)	0.4664 (4)	–0.5395 (3)	0.0190 (10)
N6	1.5310 (5)	0.2176 (5)	–0.1211 (3)	0.0320 (13)
C1	0.6217 (5)	0.1704 (5)	0.3235 (3)	0.0195 (12)
C2	0.6603 (5)	0.1502 (5)	0.3900 (3)	0.0188 (12)
H2	0.7250	0.1310	0.3929	0.023*
C3	0.6040 (5)	0.1580 (5)	0.4525 (3)	0.0195 (12)
C4	0.5090 (5)	0.1868 (5)	0.4483 (3)	0.0192 (12)
H4	0.4714	0.1929	0.4911	0.023*
C5	0.4691 (5)	0.2066 (5)	0.3814 (3)	0.0217 (12)
C6	0.5267 (5)	0.2010 (5)	0.3192 (3)	0.0193 (12)
H6	0.5024	0.2176	0.2741	0.023*
C7	0.6674 (5)	0.1505 (5)	0.2557 (3)	0.0195 (12)
C8	0.6947 (5)	0.1290 (6)	0.1973 (3)	0.0210 (12)
C9	0.7199 (5)	0.1061 (5)	0.1237 (3)	0.0192 (11)
C10	0.6472 (6)	0.1074 (6)	0.0643 (3)	0.0220 (13)
H10	0.5829	0.1258	0.0723	0.026*
C11	0.6688 (5)	0.0820 (5)	–0.0057 (3)	0.0214 (12)
H11	0.6192	0.0848	–0.0456	0.026*
C12	0.8294 (5)	0.0546 (6)	0.0365 (3)	0.0232 (13)
H12	0.8933	0.0362	0.0269	0.028*

Table continued on the next page

Table A.7.: Fractional atomic coordinates and isotropic or equivalent isotropic displacement parameters (Å^2) of the BTETP-based MOF (cont.)

	x	y	z	$U_{\text{iso}}*/U_{\text{eq}}$
C13	0.8153 (5)	0.0815 (5)	0.1086 (3)	0.0241 (13)
H13	0.8695	0.0832	0.1475	0.029*
C14	0.6423 (5)	0.1354 (5)	0.5217 (3)	0.0228 (13)
C15	0.6702 (5)	0.1160 (5)	0.5794 (3)	0.0210 (12)
C16	0.6977 (6)	0.0913 (5)	0.6501 (3)	0.0217 (13)
C17	0.7943 (6)	0.0674 (5)	0.6655 (3)	0.0228 (13)
H17	0.8462	0.0689	0.6290	0.027*
C18	0.8133 (5)	0.0417 (5)	0.7338 (3)	0.0216 (13)
H18	0.8797	0.0264	0.7436	0.026*
C19	0.6501 (5)	0.0628 (6)	0.7741 (3)	0.0229 (13)
H19	0.6008	0.0623	0.8121	0.027*
C20	0.6253 (5)	0.0894 (5)	0.7068 (3)	0.0208 (12)
H20	0.5596	0.1064	0.6989	0.025*
C21	0.3651 (6)	0.2271 (6)	0.3764 (3)	0.0233 (13)
C22	0.2751 (6)	0.2376 (5)	0.3705 (3)	0.0227 (12)
C23	0.1651 (6)	0.2492 (5)	0.3642 (3)	0.0224 (12)
C24	0.1113 (6)	0.2605 (6)	0.4272 (3)	0.0251 (13)
H24	0.1441	0.2577	0.4742	0.030*
C25	0.0086 (6)	0.2760 (6)	0.4194 (3)	0.0297 (15)
H25	−0.0282	0.2829	0.4624	0.036*
C26	0.0081 (6)	0.2668 (6)	0.2959 (4)	0.0299 (15)
H26	−0.0290	0.2667	0.2495	0.036*
C27	0.1119 (6)	0.2510 (6)	0.2969 (3)	0.0264 (13)
H27	0.1449	0.2418	0.2527	0.032*
C28	0.8819 (6)	0.3425 (5)	−0.0733 (3)	0.0215 (12)
C29	0.8315 (5)	0.3563 (5)	−0.1390 (3)	0.0186 (11)
H29	0.7659	0.3745	−0.1388	0.022*
C30	0.8780 (5)	0.3430 (5)	−0.2047 (3)	0.0198 (12)
C31	0.9732 (6)	0.3132 (5)	−0.2057 (3)	0.0220 (12)
H31	1.0044	0.3037	−0.2505	0.026*
C32	1.0214 (5)	0.2977 (5)	−0.1396 (3)	0.0205 (12)
C33	0.9769 (5)	0.3138 (5)	−0.0739 (3)	0.0223 (12)
H33	1.0113	0.3053	−0.0292	0.027*
C34	0.8419 (6)	0.3645 (6)	−0.0044 (3)	0.0242 (13)
C35	0.8149 (6)	0.3837 (6)	0.0540 (3)	0.0245 (13)
C36	0.7883 (6)	0.4076 (5)	0.1269 (4)	0.0226 (12)
C37	0.8623 (6)	0.4095 (6)	0.1878 (3)	0.0238 (13)

Table A.7.: Fractional atomic coordinates and isotropic or equivalent isotropic displacement parameters (Å^2) of the BTETP-based MOF (cont.)

	x	y	z	$U_{\text{iso}}*/U_{\text{eq}}$
H37	0.9276	0.3923	0.1807	0.029*
C38	0.8400 (6)	0.4361 (6)	0.2574 (3)	0.0246 (13)
H38	0.8904	0.4362	0.2979	0.030*
C39	0.6768 (5)	0.4594 (6)	0.2123 (3)	0.0240 (13)
H39	0.6120	0.4768	0.2209	0.029*
C40	0.6930 (5)	0.4325 (6)	0.1412 (3)	0.0242 (13)
H40	0.6397	0.4308	0.1018	0.029*
C41	0.8368 (5)	0.3667 (5)	−0.2719 (3)	0.0189 (11)
C42	0.8081 (5)	0.3886 (5)	−0.3290 (3)	0.0209 (12)
C43	0.7832 (5)	0.4132 (5)	−0.4000 (3)	0.0195 (12)
C44	0.6935 (5)	0.4462 (6)	−0.4166 (3)	0.0235 (13)
H44	0.6435	0.4506	−0.3802	0.028*
C45	0.6784 (5)	0.4719 (5)	−0.4851 (3)	0.0202 (12)
H45	0.6178	0.4949	−0.4950	0.024*
C46	0.8305 (5)	0.4319 (5)	−0.5246 (3)	0.0203 (12)
H46	0.8772	0.4257	−0.5625	0.024*
C47	0.8516 (5)	0.4055 (5)	−0.4569 (3)	0.0196 (12)
H47	0.9124	0.3822	−0.4485	0.023*
C48	1.1240 (6)	0.2742 (6)	−0.1381 (3)	0.0244 (13)
C49	1.2137 (6)	0.2624 (6)	−0.1356 (3)	0.0256 (13)
C50	1.3216 (5)	0.2483 (5)	−0.1303 (3)	0.0225 (12)
C51	1.3923 (6)	0.2633 (6)	−0.1891 (3)	0.0291 (14)
H51	660360	0.2839	−0.2334	0.035*
C52	1.4945 (6)	0.2473 (6)	−0.1811 (4)	0.0307 (15)
H52	1286386	0.2583	−0.2212	0.037*
C53	1.4647 (6)	0.2078 (6)	−0.0648 (4)	0.0301 (14)
H53	1100843	0.1915	−0.0203	0.036*
C54	1.3590 (6)	0.2198 (6)	−0.0667 (4)	0.0267 (13)
H54	451807	0.2087	−0.0255	0.032*
C55	1.7095 (6)	0.6179 (6)	−0.1235 (4)	0.0302 (14)
H55	1906933	0.6946	−0.1152	0.036*
C56	0.7818 (7)	0.8874 (7)	0.3807 (4)	0.0390 (16)
H56	0.7761	0.8095	0.3762	0.047*

Table A.8.: Atomic displacement parameters (Å^2) of the BTETP-based MOF

	U^{11}	U^{22}	U^{33}	U^{12}	U^{13}	U^{23}
Zn1	0.0195 (3)	0.0249 (4)	0.0179 (3)	0.0164 (3)	0.0014 (3)	0.0032 (3)
Zn2	0.0189 (3)	0.0245 (4)	0.0186 (3)	0.0150 (3)	0.0036 (3)	0.0042 (3)
Cl1	0.0283 (8)	0.0496 (10)	0.0265 (7)	0.0309 (8)	−0.0001 (6)	0.0009 (7)
Cl2	0.0224 (7)	0.0239 (7)	0.0248 (7)	0.0135 (6)	0.0028 (6)	0.0047 (6)
Cl3	0.0206 (7)	0.0282 (8)	0.0240 (7)	0.0123 (6)	0.0052 (5)	0.0035 (6)
Cl4	0.0239 (7)	0.0403 (9)	0.0299 (8)	0.0242 (7)	0.0057 (6)	0.0084 (7)
Cl5	0.0650 (14)	0.0508 (13)	0.0400 (10)	0.0276 (11)	0.0201 (9)	0.0121 (9)
Cl6	0.0312 (9)	0.0473 (11)	0.0338 (9)	0.0170 (8)	0.0006 (7)	0.0014 (8)
Cl7	0.0362 (10)	0.0450 (11)	0.0423 (10)	0.0259 (9)	−0.0046 (8)	0.0060 (8)
Cl8	0.0711 (17)	0.0769 (18)	0.0520 (13)	0.0372 (15)	−0.0208 (12)	−0.0045 (12)
Cl9	0.0429 (10)	0.0503 (12)	0.0409 (10)	0.0341 (9)	0.0048 (8)	0.0053 (9)
Cl10	0.0466 (13)	0.0589 (15)	0.0651 (14)	0.0175 (11)	0.0167 (10)	0.0167 (11)
N1	0.017 (2)	0.024 (3)	0.023 (2)	0.013 (2)	0.0024 (19)	0.002 (2)
N2	0.017 (2)	0.024 (3)	0.019 (2)	0.013 (2)	0.0031 (18)	0.004 (2)
N3	0.028 (3)	0.041 (4)	0.031 (3)	0.024 (3)	0.002 (2)	0.003 (2)
N4	0.020 (3)	0.022 (3)	0.022 (2)	0.011 (2)	0.0057 (19)	0.004 (2)
N5	0.018 (2)	0.023 (3)	0.024 (2)	0.016 (2)	0.0019 (19)	0.0035 (19)
N6	0.033 (3)	0.036 (3)	0.036 (3)	0.025 (3)	0.003 (3)	−0.001 (3)
C1	0.016 (3)	0.026 (3)	0.019 (3)	0.011 (3)	0.003 (2)	0.000 (2)
C2	0.016 (3)	0.016 (3)	0.025 (3)	0.008 (2)	0.001 (2)	0.003 (2)
C3	0.020 (3)	0.018 (3)	0.021 (3)	0.009 (3)	0.000 (2)	0.005 (2)
C4	0.017 (3)	0.021 (3)	0.020 (3)	0.008 (3)	0.004 (2)	0.002 (2)
C5	0.020 (3)	0.028 (3)	0.026 (3)	0.019 (3)	0.004 (2)	0.005 (2)
C6	0.017 (3)	0.020 (3)	0.022 (3)	0.009 (3)	0.003 (2)	0.005 (2)
C7	0.021 (3)	0.024 (3)	0.019 (3)	0.015 (3)	0.000 (2)	0.003 (2)
C8	0.016 (3)	0.026 (3)	0.025 (3)	0.013 (3)	0.001 (2)	0.005 (2)
C9	0.019 (3)	0.020 (3)	0.020 (3)	0.011 (2)	0.001 (2)	−0.001 (2)
C10	0.023 (3)	0.029 (3)	0.024 (3)	0.021 (3)	0.002 (2)	0.003 (2)
C11	0.020 (3)	0.027 (3)	0.026 (3)	0.017 (3)	0.002 (2)	0.006 (2)
C12	0.017 (3)	0.037 (4)	0.021 (3)	0.018 (3)	0.001 (2)	0.001 (3)
C13	0.021 (3)	0.034 (4)	0.024 (3)	0.017 (3)	0.001 (2)	0.005 (2)
C14	0.023 (3)	0.024 (3)	0.023 (3)	0.012 (3)	0.004 (2)	0.001 (2)
C15	0.019 (3)	0.021 (3)	0.024 (3)	0.009 (3)	0.005 (2)	0.007 (2)
C16	0.024 (3)	0.022 (3)	0.021 (3)	0.013 (3)	0.000 (2)	0.004 (2)
C17	0.025 (3)	0.024 (3)	0.022 (3)	0.013 (3)	0.005 (2)	0.003 (2)
C18	0.022 (3)	0.031 (4)	0.021 (3)	0.019 (3)	0.007 (2)	0.005 (2)
C19	0.020 (3)	0.029 (3)	0.028 (3)	0.017 (3)	0.008 (2)	0.006 (2)

Table A.8.: Atomic displacement parameters (Å^2) of BTETP-based MOF (cont.)

	U^{11}	U^{22}	U^{33}	U^{12}	U^{13}	U^{23}
C20	0.018 (3)	0.023 (3)	0.026 (3)	0.013 (3)	0.003 (2)	0.005 (2)
C21	0.026 (3)	0.033 (4)	0.021 (3)	0.021 (3)	0.006 (2)	0.005 (3)
C22	0.029 (3)	0.023 (3)	0.023 (3)	0.018 (3)	0.003 (3)	0.002 (3)
C23	0.024 (3)	0.024 (3)	0.027 (3)	0.017 (3)	0.003 (2)	0.005 (3)
C24	0.027 (3)	0.032 (4)	0.023 (3)	0.020 (3)	0.003 (2)	0.003 (3)
C25	0.032 (4)	0.045 (4)	0.024 (3)	0.030 (3)	0.003 (3)	0.000 (3)
C26	0.032 (4)	0.043 (4)	0.024 (3)	0.025 (3)	0.001 (3)	0.005 (3)
C27	0.026 (3)	0.030 (4)	0.027 (3)	0.016 (3)	0.007 (2)	0.006 (3)
C28	0.025 (3)	0.026 (3)	0.018 (3)	0.015 (3)	0.006 (2)	0.006 (2)
C29	0.016 (3)	0.016 (3)	0.021 (3)	0.005 (2)	0.001 (2)	0.000 (2)
C30	0.024 (3)	0.018 (3)	0.021 (3)	0.012 (3)	0.004 (2)	0.004 (2)
C31	0.028 (3)	0.026 (3)	0.017 (3)	0.017 (3)	0.002 (2)	0.000 (2)
C32	0.023 (3)	0.017 (3)	0.024 (3)	0.011 (3)	0.003 (2)	0.005 (2)
C33	0.020 (3)	0.026 (3)	0.021 (3)	0.010 (3)	−0.001 (2)	0.005 (2)
C34	0.025 (3)	0.025 (3)	0.022 (3)	0.012 (3)	0.000 (2)	0.002 (2)
C35	0.028 (3)	0.022 (3)	0.020 (3)	0.009 (3)	0.003 (2)	0.001 (2)
C36	0.024 (3)	0.013 (3)	0.028 (3)	0.006 (2)	0.006 (3)	0.002 (2)
C37	0.026 (3)	0.024 (3)	0.028 (3)	0.016 (3)	0.006 (3)	0.002 (3)
C38	0.030 (3)	0.030 (4)	0.024 (3)	0.024 (3)	−0.001 (2)	0.001 (2)
C39	0.016 (3)	0.030 (4)	0.027 (3)	0.012 (3)	−0.002 (2)	0.001 (3)
C40	0.019 (3)	0.034 (4)	0.020 (3)	0.013 (3)	0.001 (2)	0.005 (2)
C41	0.018 (3)	0.015 (3)	0.024 (3)	0.008 (2)	0.006 (2)	0.003 (2)
C42	0.015 (3)	0.025 (3)	0.025 (3)	0.011 (3)	0.005 (2)	0.002 (2)
C43	0.018 (3)	0.021 (3)	0.020 (3)	0.010 (3)	0.003 (2)	0.002 (2)
C44	0.020 (3)	0.033 (4)	0.025 (3)	0.017 (3)	0.006 (2)	0.007 (3)
C45	0.015 (3)	0.025 (3)	0.027 (3)	0.013 (3)	0.006 (2)	0.008 (2)
C46	0.016 (3)	0.022 (3)	0.025 (3)	0.012 (3)	0.004 (2)	0.001 (2)
C47	0.013 (3)	0.019 (3)	0.028 (3)	0.008 (2)	0.005 (2)	0.006 (2)
C48	0.025 (3)	0.029 (4)	0.021 (3)	0.015 (3)	0.001 (2)	0.002 (2)
C49	0.026 (3)	0.028 (4)	0.026 (3)	0.015 (3)	0.002 (2)	0.005 (3)
C50	0.022 (3)	0.023 (3)	0.025 (3)	0.014 (3)	0.000 (2)	0.000 (2)
C51	0.031 (4)	0.039 (4)	0.023 (3)	0.021 (3)	0.003 (3)	0.003 (3)
C52	0.030 (4)	0.037 (4)	0.028 (3)	0.018 (3)	0.006 (3)	0.001 (3)
C53	0.032 (4)	0.035 (4)	0.030 (3)	0.022 (3)	0.000 (3)	0.004 (3)
C54	0.022 (3)	0.031 (4)	0.033 (3)	0.017 (3)	0.007 (2)	0.006 (3)
C55	0.034 (4)	0.034 (4)	0.032 (3)	0.025 (3)	0.001 (3)	0.000 (3)
C56	0.038 (4)	0.032 (4)	0.050 (4)	0.018 (3)	0.008 (3)	0.010 (3)

Table A.9.: Geometric parameters (Å, °) of the BTETP-based MOF

Zn1–N2^{i}	2.030 (5)	C45–N5–Zn2^{i}	119.6 (4)	C43–C47	1.405 (8)
Zn1–N1	2.046 (5)	C46–N5–Zn2^{i}	121.3 (4)	C44–C45	1.364 (8)
Zn1–Cl1	2.2095 (15)	C53–N6–C52	115.8 (5)	C46–C47	1.371 (8)
Zn1–Cl2	2.2519 (17)	C2–C1–C6	120.2 (5)	C48–C49	1.194 (9)
Zn2–N5^{ii}	2.039 (5)	C2–C1–C7	121.9 (5)	C49–C50	1.436 (8)
Zn2–N4	2.043 (5)	C6–C1–C7	117.6 (5)	C50–C54	1.387 (9)
Zn2–Cl4	2.2228 (15)	C1–C2–C3	120.0 (5)	C50–C51	1.399 (9)
Zn2–Cl3	2.2509 (17)	C2–C3–C4	120.0 (5)	C51–C52	1.384 (9)
Cl5–C55	1.752 (8)	C2–C3–C14	120.5 (5)	C53–C54	1.394 (8)
Cl6–C55	1.765 (7)	C4–C3–C14	119.6 (5)	C19–C20–C16	119.6 (5)
Cl7–C55	1.770 (6)	C3–C4–C5	120.3 (5)	C22–C21–C5	176.1 (7)
Cl8–C56	1.745 (8)	C6–C5–C4	119.8 (5)	C21–C22–C23	179.0 (7)
Cl9–C56	1.768 (8)	C6–C5–C21	120.4 (5)	C27–C23–C24	118.6 (5)
Cl10–C56	1.746 (8)	C4–C5–C21	119.8 (5)	C27–C23–C22	121.6 (6)
N1–C12	1.346 (7)	C5–C6–C1	119.7 (5)	C24–C23–C22	119.8 (6)
N1–C11	1.351 (7)	C8–C7–C1	174.2 (6)	C25–C24–C23	118.2 (6)
N2–C19	1.352 (7)	C7–C8–C9	174.8 (6)	N3–C25–C24	124.2 (6)
N2–C18	1.353 (7)	C10–C9–C13	117.6 (5)	N3–C26–C27	124.5 (6)
N2–Zn1^{ii}	2.030 (5)	C10–C9–C8	119.6 (5)	C23–C27–C26	118.0 (6)
N3–C26	1.323 (8)	C13–C9–C8	122.7 (5)	C33–C28–C29	120.1 (5)
N3–C25	1.339 (8)	C11–C10–C9	119.6 (5)	C33–C28–C34	119.3 (5)
N4–C39	1.352 (7)	N1–C11–C10	123.2 (5)	C29–C28–C34	120.5 (5)
N4–C38	1.354 (7)	N1–C12–C13	123.3 (5)	C30–C29–C28	119.6 (5)
N5–C45	1.352 (7)	C12–C13–C9	119.1 (5)	C29–C30–C31	120.5 (5)
N5–C46	1.357 (7)	C15–C14–C3	177.8 (6)	C29–C30–C41	121.3 (5)
N5–Zn2^{i}	2.039 (5)	C14–C15–C16	177.0 (6)	C31–C30–C41	118.0 (5)
N6–C53	1.333 (9)	C17–C16–C20	117.5 (5)	C32–C31–C30	119.3 (5)
N6–C52	1.335 (9)	C17–C16–C15	122.7 (6)	C33–C32–C31	120.1 (5)
C1–C2	1.387 (8)	C20–C16–C15	119.8 (5)	C33–C32–C48	119.2 (5)
C1–C6	1.414 (8)	C18–C17–C16	119.5 (5)	C31–C32–C48	120.6 (5)
C1–C7	1.446 (7)	N2–C18–C17	123.1 (5)	C32–C33–C28	120.4 (5)
C2–C3	1.394 (8)	N2–C19–C20	122.4 (5)	C35–C34–C28	176.4 (7)
C3–C4	1.399 (8)	C10–C11	1.370 (8)	C34–C35–C36	176.9 (7)
C3–C14	1.444 (8)	C12–C13	1.380 (8)	C40–C36–C37	117.1 (5)
C4–C5	1.399 (8)	C14–C15	1.188 (9)	C40–C36–C35	123.2 (6)
C5–C6	1.392 (8)	C15–C16	1.435 (8)	C37–C36–C35	119.6 (5)
C5–C21	1.439 (7)	C16–C17	1.398 (8)	C38–C37–C36	119.9 (5)
C7–C8	1.190 (8)	C16–C20	1.406 (8)	N4–C38–C37	122.5 (6)
C8–C9	1.438 (8)	C17–C18	1.371 (8)	N4–C39–C40	122.9 (5)

Table continued on the next page

Table A.9.: Geometric parameters (Å, °) of the BTETP-based MOF (cont.)

C9–C10	1.392 (8)	C19–C20	1.378 (8)	C39–C40–C36	119.7 (5)
C9–C13	1.399 (7)	C21–C22	1.191 (8)	C42–C41–C30	176.7 (6)
N2^i–Zn1–N1	117.98 (19)	C22–C23	1.445 (8)	C41–C42–C43	174.5 (6)
N2^i–Zn1–Cl1	108.29 (13)	C23–C27	1.384 (9)	C44–C43–C47	117.0 (5)
N1–Zn1–Cl1	109.96 (14)	C23–C24	1.395 (8)	C44–C43–C42	123.5 (5)
N2^i–Zn1–Cl2	104.37 (15)	C24–C25	1.385 (8)	C47–C43–C42	119.5 (5)
N1–Zn1–Cl2	101.90 (15)	C26–C27	1.398 (8)	C45–C44–C43	119.8 (5)
Cl1–Zn1–Cl2	114.35 (7)	C28–C33	1.396 (8)	N5–C45–C44	123.2 (5)
N5^{ii}–Zn2–N4	117.5 (2)	C28–C29	1.401 (8)	N5–C46–C47	122.6 (5)
N5^{ii}–Zn2–Cl4	108.32 (13)	C28–C34	1.435 (8)	C46–C47–C43	119.8 (5)
N4–Zn2–Cl4	109.36 (14)	C29–C30	1.394 (8)	C49–C48–C32	175.6 (7)
N5^{ii}–Zn2–Cl3	103.86 (15)	C30–C31	1.409 (8)	C48–C49–C50	178.3 (7)
N4–Zn2–Cl3	102.89 (15)	C30–C41	1.433 (8)	C54–C50–C51	117.9 (5)
Cl4–Zn2–Cl3	115.02 (7)	C31–C32	1.403 (8)	C54–C50–C49	121.1 (6)
C12–N1–C11	117.1 (5)	C32–C33	1.391 (8)	C51–C50–C49	121.0 (6)
C12–N1–Zn1	118.3 (4)	C32–C48	1.446 (8)	C52–C51–C50	118.4 (6)
C11–N1–Zn1	122.5 (4)	C34–C35	1.179 (8)	N6–C52–C51	124.8 (6)
C19–N2–C18	117.9 (5)	C35–C36	1.436 (9)	N6–C53–C54	124.7 (6)
C19–N2–Zn1^{ii}	121.4 (4)	C36–C40	1.397 (8)	C50–C54–C53	118.4 (6)
C18–N2–Zn1^{ii}	120.0 (4)	C36–C37	1.407 (9)	Cl5–C55–Cl6	109.9 (4)
C26–N3–C25	116.4 (5)	C37–C38	1.368 (8)	Cl5–C55–Cl7	110.7 (4)
C39–N4–C38	117.7 (5)	C39–C40	1.370 (8)	Cl6–C55–Cl7	110.4 (3)
C39–N4–Zn2	119.0 (4)	C41–C42	1.199 (8)	Cl8–C56–Cl10	110.9 (5)
C38–N4–Zn2	121.3 (4)	C42–C43	1.429 (8)	Cl8–C56–Cl9	109.3 (4)
C45–N5–C46	117.4 (5)	C43–C44	1.403 (8)	Cl10–C56–Cl9	111.2 (4)